Strathclyde Engagement with the UK National HVDC Centre: Phase I Converter and GB Network Modelling

Doc. Type:	Technical report	*Date:*	**24/08/2018**
Doc. Nº:	**USTRATH-HVDC Centre-P1-002**	*Issue:* **3**	*Page:* **1** *of* **27**
Title:	Validation of Real-time User-defined MMC Models		

	Name&Function	*Signature*	*Date*
Prepared by:	Deyang Guo, Md Habibur Rahman, Grain. P Adam, Abdullah Emhemed		20/08/2018
Approved by:	Lie Xu		24/08/2018
Authorized by:	Yash Audichya		

DISTRIBUTION LIST	N	A	I
Internal			
External			

N=Number of copy
A=Application
I=Information

TABLE OF CONTENT

Executive summary

This report presents a one-to-one validation of a number of real-time half-bridge modular multilevel converter (HB-MMC) models, namely, the switching function and averaged against offline switching function HB-MMC model. The user-defined real-time and offline simulation models employed in this report, in RTDS/RSCAD and PSCAD/EMTDC underpinned by theoretical basis described in the previous report[1] on fundamentals and synthesis of different models of a modular multilevel voltage source converter and use identical parameters and controllers, and with both sets are extensively tested under a range of identical operating conditions and ac and DC network faults. From detailed corroboration presented in this report, it has been shown that the real-time averaged and switching function HB-MMC models produce near identical results as the offline switching function HB-MMC (extensively validated against other equivalent offline models in the previous report[1]). Despite the minor differences and limitations of the RTDS platform, the margins of the errors between the results of the real-time and offline simulation are negligible (less than 1%) during steady-state, symmetrical and asymmetrical AC faults, and DC faults.

[1] TR on Modular Multilevel Voltage Source Converter: Fundamentals and Synthesis of Different Models, Strathclyde-UK National HVDC Centre collaborative research project, TR ref. USTRATH-HVDC Centre-P1-001, April 2018.

1 Introduction

In the early 2000s, significant efforts were invested in addressing the shortcomings of traditional multilevel voltage source converter (VSC) topologies, with particular emphasis on the scalability to high power and operating voltages suitable for transmission applications, generation of high quality output AC voltage with virtually zero harmonics and extremely low dv/dt, and improved reliability. These efforts have resulted in the development of the modular multilevel converter (MMC) and its derivatives [1-3], which are able to achieve the aforementioned objectives. Compared to traditional VSC topologies, MMC offers significant further advantages such as high availability, ease of failure management, and extremely low semiconductor losses, which can be further minimized by engineering optimization of the switching devices. However, a large number of cell capacitors and switching elements in each arm of the MMC present significant simulation challenges, computationally and memory wise [4-8].

As a follow up of the previous report that has presented extensive offline validations of a number of MMC models, namely, the switching function, and Thevenin equivalent and averaged MMC models, this report presents detailed validations of user-defined real-time MMC switching function and averaged MMC models developed in RSCAD against the offline PSCAD MMC switching function models. For one-to-one validation, the switching function MMC models in both platforms (PSCAD and RSCAD) have 20 cells per arm, with identical controllers and parameters. These offline and real-time simulation results show that the developed MMC models are practically equivalent and able to replicate the typical behaviour of the MMC under normal operation and AC and DC network faults.

2 Real-time Simulation Models

Fig. 1 depicts a generic layout of the developed MMC model using real-time digital simulation (RTDS) dual time step technique. The MMC models with the requirements of high switching frequency are built in small time step (i.e. 1.4-2.5μs), whilst the AC grid source is modelled in a larger time step (i.e. 50 μs).

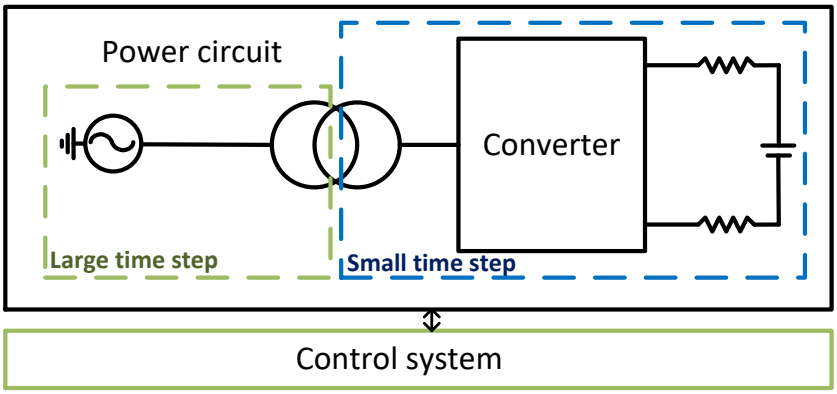

Fig. 1: A single terminal MMC system modelling method in RTDS

2.1 Power Circuit and Control System Modelling

On the basis of detailed discussions of the MMC modelling presented in the previous report [9], real-time user defined 20-cell switching function and averaged half-bridge MMC models are developed using

RSCAD-RTDS simulation platform. The developed models in this report are validated against an offline 20-cell half-bridge MMC switching function model developed in PSCAD-EMTDC has been validated in previous studies [9]. For simplicity and also adequacy of the model for system studies, 20-cell per arm are considered. The number of cells in the developed RSCAD-RTDS model can be easily scaled and modified if more details are required and sufficient RTDS modelling hardware are available.

The RTDS switching function and averaged HB-MMC models as shown in Fig. 2 and Fig. 3 consist of two parts:

- The power circuit part which includes controllable voltage sources, arm inductors and IGBTs and diodes being used to mimic the half-bridge MMC blocking state.
- The calculation part that simulates the half-bridge MMC cell dynamics and generates the upper and lower arm voltages V_{armU} and V_{armL}.

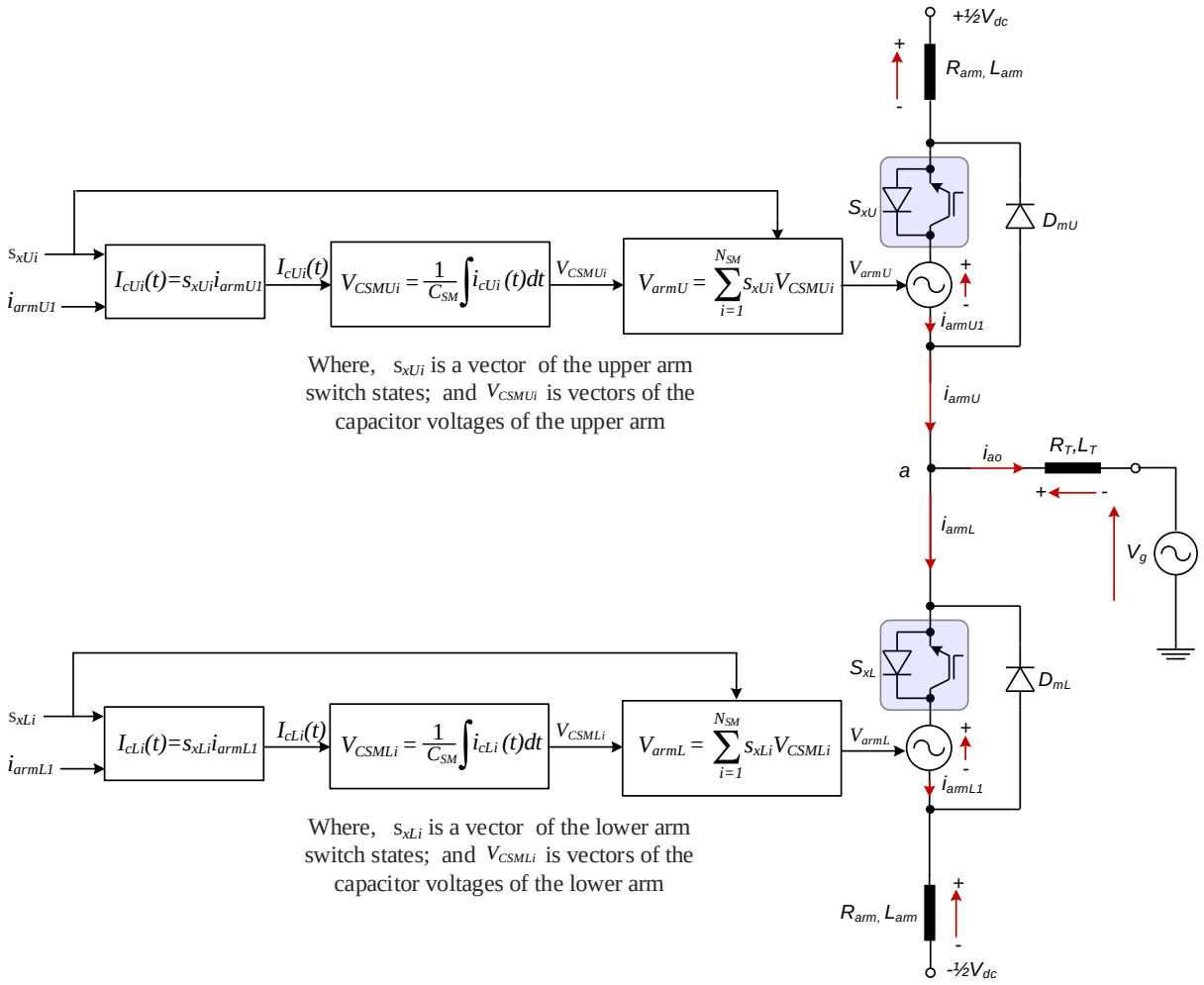

Fig. 2 Graphical depiction of the MMC switching function model

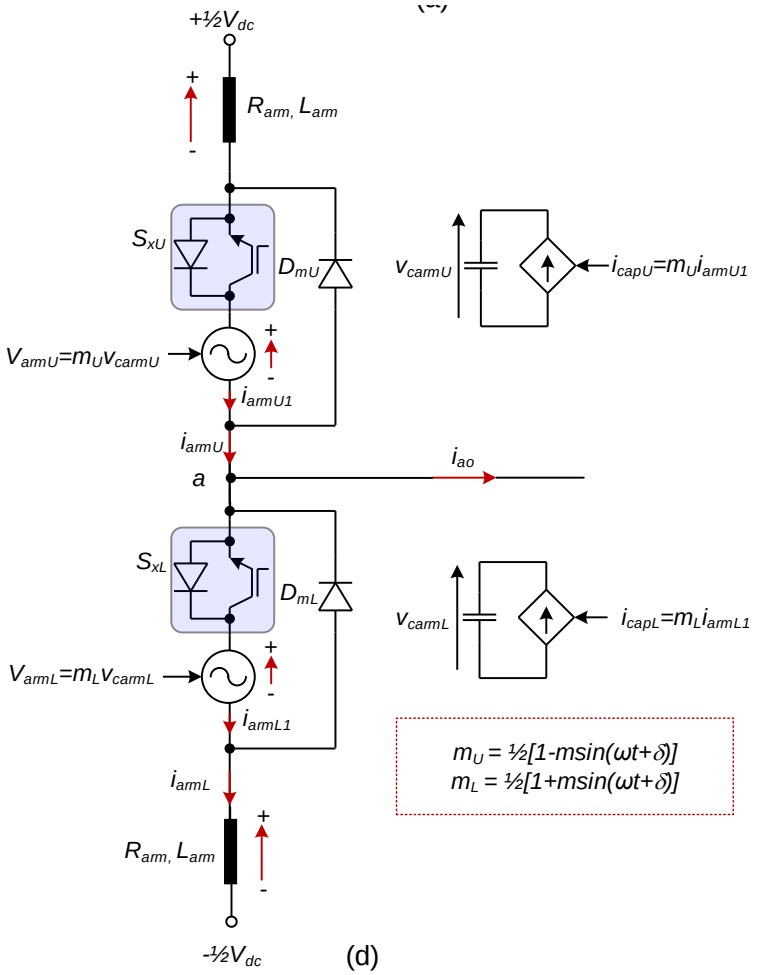

Fig. 3: Modular multilevel converter per arm averaged model

In RTDS platform, the power circuit part of the MMC switching function and averaged HB-MMC models and its associated components such as the DC side circuit and interfacing transformer are placed in a dedicated small time step template called “VSC bridges” available in RSCAD library and ranging from 1.4µs to 2.5µs. While the part that calculates the cell capacitor dynamics and control systems are placed in a dedicated large time-step template of 50µs. The user-defined components that implement calculations of cell capacitor dynamics and voltage balancing are realised in MATLAB-SIMULINK and then converted to RSCAD using code generation with the help of real-time embedded coder that can optimise the generated code for a number of objectives such code efficiency, RAM usage, traceability, etc. The whole real-time simulation model of the test system is implemented on one RTDS rack, with a PB5 card with two processors and three GPC cards (two processors each). Both processors on the PB5 card are assigned to solve the power circuit that operates at a small time step, and with calculation part of each phase on one GPC processor. Since this report aims to validate the MMC behaviours under a number of operating conditions, the DC side of the half-bridge MMC is modelled by stiff DC voltage source and one pi-section per DC pole. While the AC side is placed outside of the small-time step bridge and it adopts large simulation time-

step of 50μs. The connection between the AC system that operates at large time-step and the MMC power circuit and its DC side components which operate at small time-step is realised by using a VSC interface transformer from the RSCAD small time-step library.

2.2 Modelling Challenges

As described above, the real-time simulation model of the overall system is implemented on one RTDS rack that consists of a PB5 card (with 2 PB5 processors) and 3 GPC cards (6 GPC processors). The first processor on the PB5 card is assigned for general large time step network solution, the second PB5 processor is assigned to solve the power circuits of the MMC and DC side that operate at small-time step. The control systems and AC side network power circuits which both operate at large time-step are assigned to two separate GPC processors. So, in the existing RTDS architecture being used to produce the results in this report, the small time step box limits the maximum number of electrical nodes in the power circuit that operates at small time-step, while that of a single processor determines the maximum number of MMC cells could be simulated.

Generally, the two platforms use slightly different approaches in the modelling of some electrical components. For example, switching devices are modelled in different ways and the primary and secondary winding configurations of the interface transformer in RTDS are different compared to the transformer model in PSCAD. Considering such small modelling differences between the offline and real-time simulation platforms, some small mismatch in the simulation results between the two models may exist.

Table 1 Test system parameters

Parameters		**Value**
MMC rated apparent power (Sn)		1265MVA
MMC rated active power (P)		±1200MW
MMC rated reactive power(Q)		±400MVAr
MMC nominal DC Voltage (V_{dc})		640kV(±320kV)
MMC rated AC output voltage (L-L)		360kV
Arm inductance (L_{arm})		0.13pu
Cell capacitance (C_{SM})	20-cell MMC	628μF
	Averaged model	31.4μF
Nominal Frequency		50Hz
Transformer rated apparent power		1265MVA
Interfacing transformer voltage ratio		400/360kV
Transformer leakage reactance		0.18pu
Transformer resistance		0.004452pu

3 Test system

This section uses one converter terminal of the MMC based point-to-point HVDC link to validate the real-time user defined averaged and switching function HB-MMC models against the offline switching function model, which has been previously validated. The system in Fig. 4 is modelled in PSCAD and RTDS, with full sets of controllers described in previous report [9]. Detailed system parameters are listed

in Table 1. The cell capacitances of the 20-cell switching function and averaged HB-MMC models are calculated, assuming the same minimum inertia constant of 30ms (or 30kJ/MVA). In this report, high impedance AC side grounding is adopted to define insulation level of the DC side.

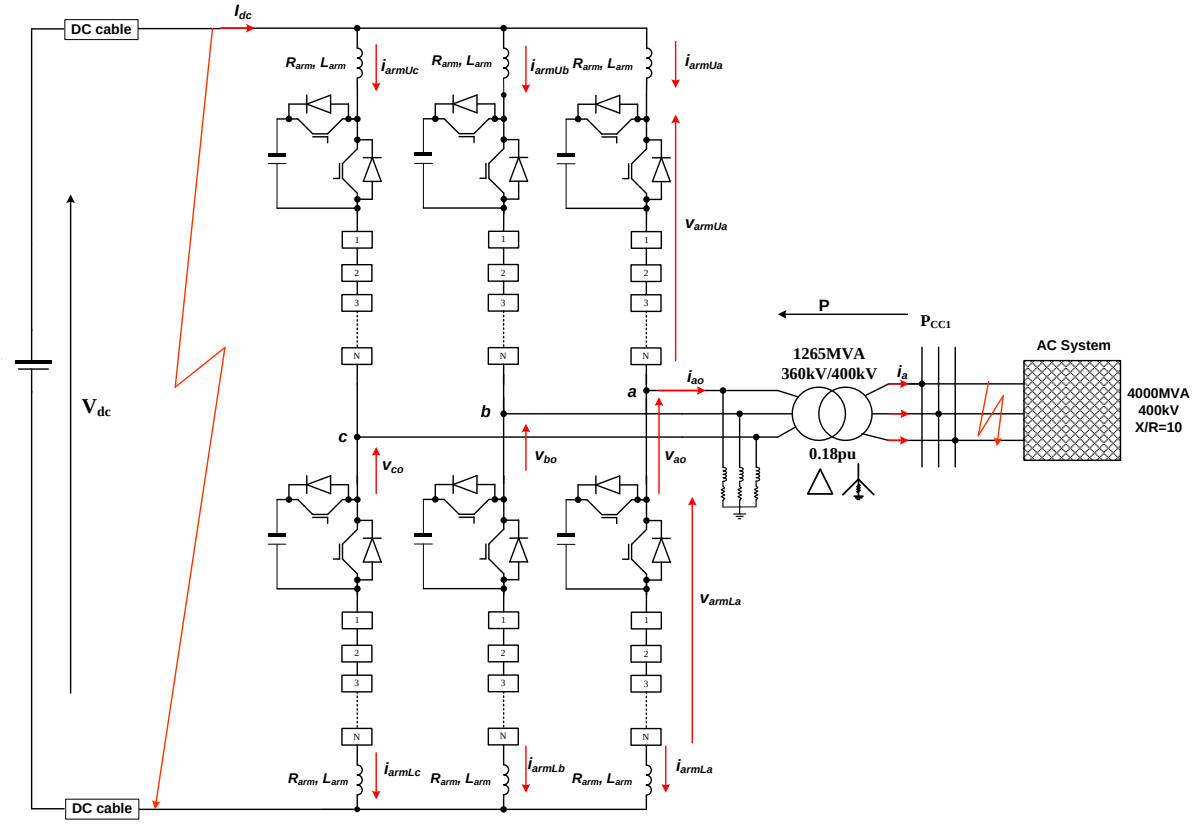

Fig. 4: Illustrative test system (power, current and voltage polarities in this figure are assumed to be positive)

4 Validation of Real-Time Simulation Models against Off-Line Equivalent

It has been proven that the MMCs with reduced number of cells per arm (20 cells Thevenin equivalent and switching function models) and averaged MMC model are capable of reproducing the typical behaviour of MMCs with large number of cells per arm (350 cells Thevenin equivalent and switching function models), with negligible errors [9]. Also, it has been established that the average and switching function MMC models offer the fastest simulation times, without significant sacrifice in the accuracy of the results in wide range of system-level studies including symmetrical and asymmetrical AC faults, and DC faults. Therefore, this section presents detailed validation of the real-time MMC simulation models, namely, the 20-cell switching function and averaged models against offline PSCAD 20-cell switching models. Moreover, it has been shown in [9] that neither the operating conditions, e.g. active/reactive power, system strength, nor MMC operating mode, e.g. power control, AC voltage control, do not invalidate or lead to divergence of the models. On this ground, most of the studies are conducted with the main scenario of

strong AC grid (SCR=10) and when MMC operates with rated active and reactive powers of 1200 MW and 400 MVAr inductive.

The operating conditions for all fault cases in this section are summarised as follows:

- In the pre-fault, during fault and post-fault conditions, the rated active and reactive powers exchange between the MMC and AC grid are 1200 MW and 400 MVAr respectively. The power flow from AC toward the converter is assumed as the positive direction.
- All fault studies are performed as successive events as summarized below:
  - At *t*=2s, a temporary solid single-phase-to-ground AC fault is applied at the point of common-coupling (PCC_1), with 300ms fault duration.
  - At *t*=4s, a temporary solid symmetrical three-phase-to-ground AC fault is applied at PCC_1, with 300ms fault duration.
  - At *t*=5s, a temporary solid phase-to-phase AC fault is applied at PCC_1, with 300ms fault duration.
  - At *t*=6s, a permanent pole-to-pole DC short circuit fault is applied in the DC side and converter blocking is activated after 50μs from fault inception.
  - In another case at *t*=3s, a permanent pole-to-ground DC short circuit fault is applied in the DC side and converter blocking is activated after 50μs from fault inception.
  - In a case operate in a weak AC grid (SCR=3), at *t*=4s, a temporary solid symmetrical three-phase-to-ground AC fault is applied at PCC_1, with 300ms fault duration.

4.1 Single-Phase-to-Ground AC Fault

Fig. 5 displays simulation waveforms for a single-phase-to-ground AC fault. Fig. 5(a) and (b), (c) and (d), and (e) and (f) show full-scaled and zoomed simulation waveforms for three-phase AC voltages at PCC, three-phase AC currents MMC injects into PCC, and three-phase AC current the MMC injects into low-voltage side of the interfacing transformer (converter side currents). The zoomed waveforms are captured around the instant of fault inception. These waveforms show that the real-time waveforms of the 20-cell switching function and average models are identical, and both exhibit negligible errors in the first few peaks of the AC side currents (grid and converter sides). Similarly, the plots for the upper and lower arm currents displayed in Fig. 5 (g) and (h), and (i) and (j) also show small and brief errors in the first few peaks of the arm current following AC fault inception, and quickly the errors between the offline and real-time models have disappeared. The plots for the sums of the upper and lower cell capacitors of the three models being compared in Fig. 5 (k) to (m) indicate that the real-time and offline simulations exhibit similar behaviours and match well during steady-state and transients. Fig. 5(o), (p) and (q) show that the real-time and offline simulation waveforms for the active and reactive powers and DC link current during single-phase AC fault are similar, with small errors appear in the reactive power during fault period. Detailed investigation of the errors observed between the reactive powers of the PSCAD and RTDS reveals that the interfacing transformer model in RSCAD is the main cause. For the same transformer parameters, the measured reactive power consumptions of the interfacing transformers are different in the two platforms (PSCAD and RSCAD), with PSCAD exhibits a slightly higher reactive power consumption. Further investigation at control system level also show that during steady-state condition, the PSCAD and RSCAD achieve the

same reactive power of 400MVAr by slightly different quadrature currents (i_q), with magnitudes of the errors between the two platforms are less than 20A.

The results of the detailed validation of the real-time and offline simulation shown in Fig. 5 confirm the suitability of the presented real-time user-defined MMC models (20-cell switching function and averaged) for studying single-phase-to-ground AC faults.

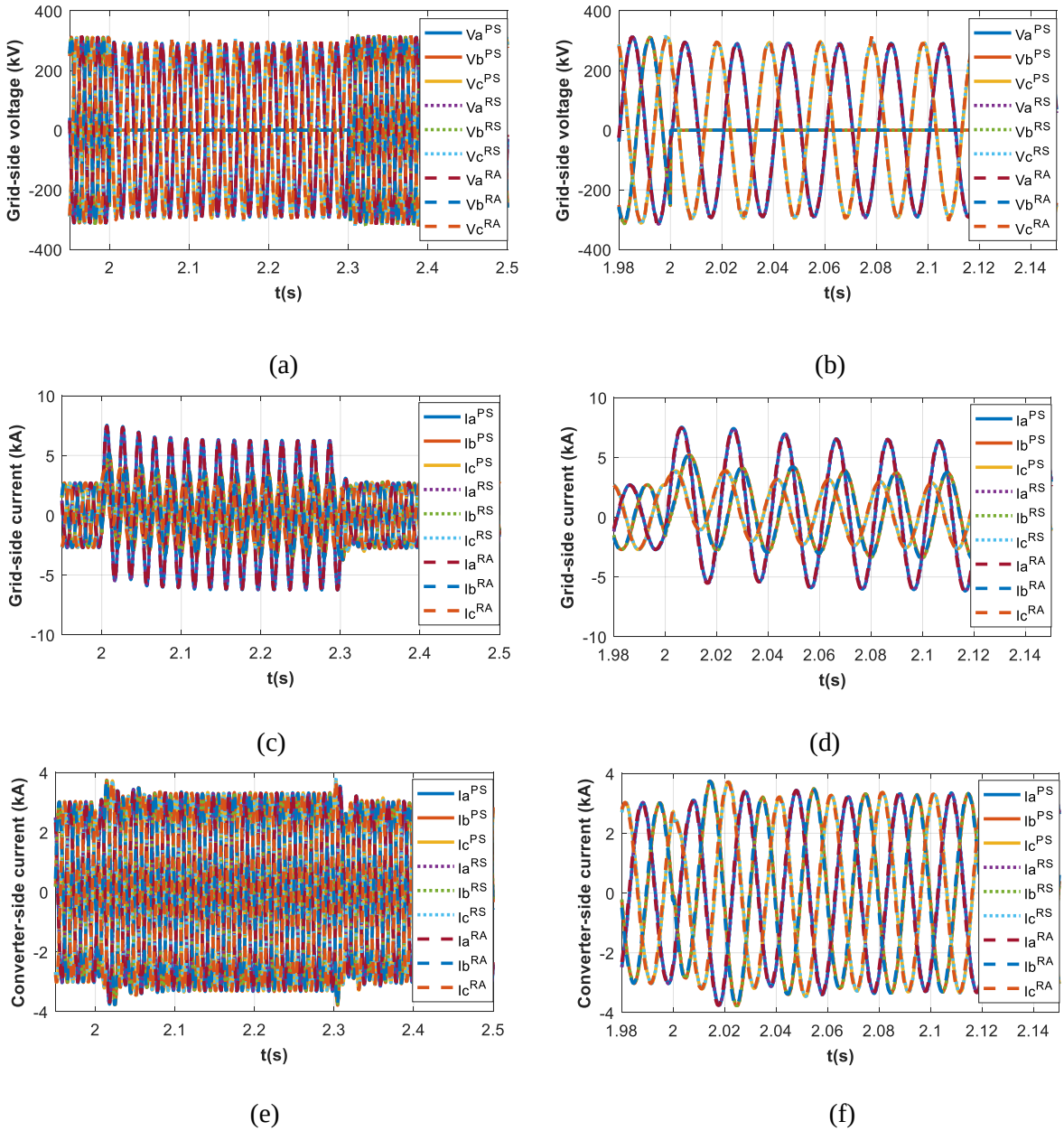

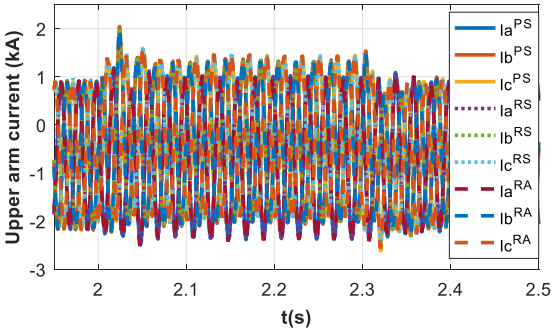
Upper arm current (kA)
t(s)
Ia^PS
Ib^PS
Ic^PS
Ia^RS
Ib^RS
Ic^RS
Ia^RA
Ib^RA
Ic^RA

(g)

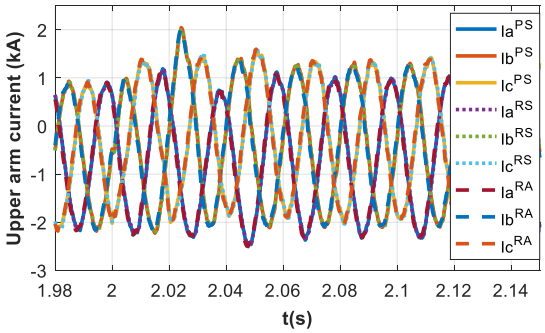
Upper arm current (kA)
t(s)
Ia^PS
Ib^PS
Ic^PS
Ia^RS
Ib^RS
Ic^RS
Ia^RA
Ib^RA
Ic^RA

(h)

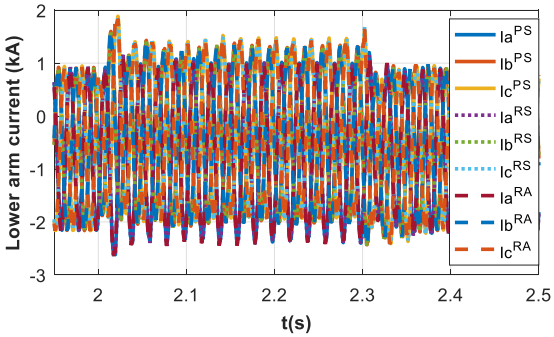
Lower arm current (kA)
t(s)
Ia^PS
Ib^PS
Ic^PS
Ia^RS
Ib^RS
Ic^RS
Ia^RA
Ib^RA
Ic^RA

(i)

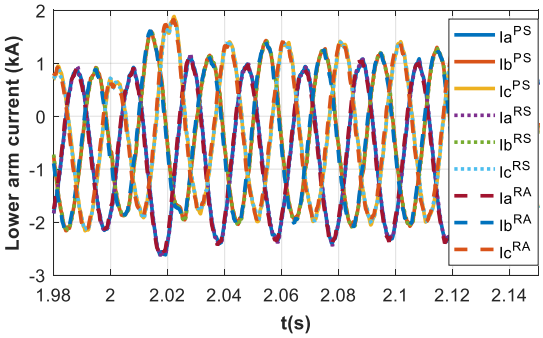
Lower arm current (kA)
t(s)
Ia^PS
Ib^PS
Ic^PS
Ia^RS
Ib^RS
Ic^RS
Ia^RA
Ib^RA
Ic^RA

(j)

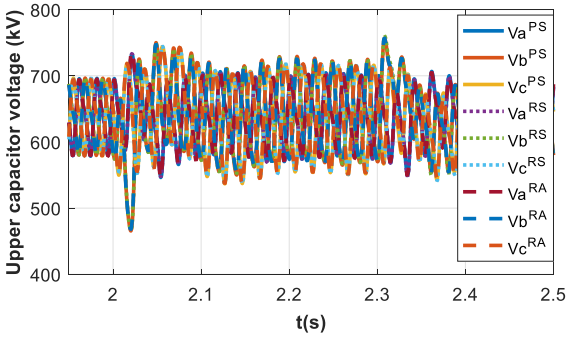
Upper capacitor voltage (kV)
t(s)
Va^PS
Vb^PS
Vc^PS
Va^RS
Vb^RS
Vc^RS
Va^RA
Vb^RA
Vc^RA

(k)

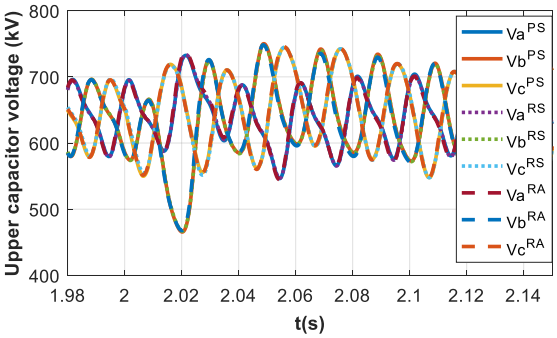
Upper capacitor voltage (kV)
t(s)
Va^PS
Vb^PS
Vc^PS
Va^RS
Vb^RS
Vc^RS
Va^RA
Vb^RA
Vc^RA

(l)

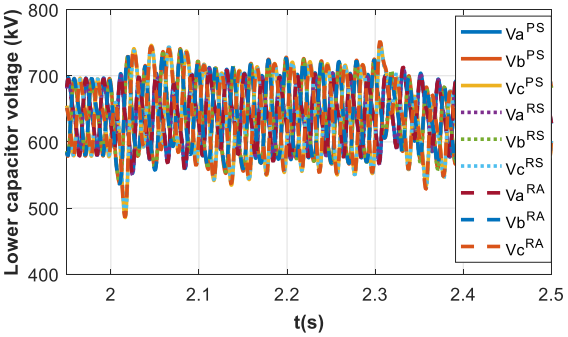
Lower capacitor voltage (kV)
t(s)
Va^PS
Vb^PS
Vc^PS
Va^RS
Vb^RS
Vc^RS
Va^RA
Vb^RA
Vc^RA

(m)

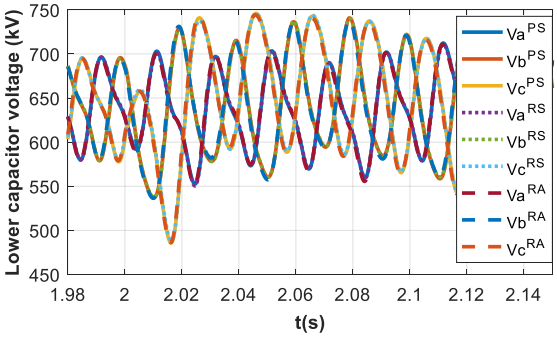
Lower capacitor voltage (kV)
t(s)
Va^PS
Vb^PS
Vc^PS
Va^RS
Vb^RS
Vc^RS
Va^RA
Vb^RA
Vc^RA

(n)

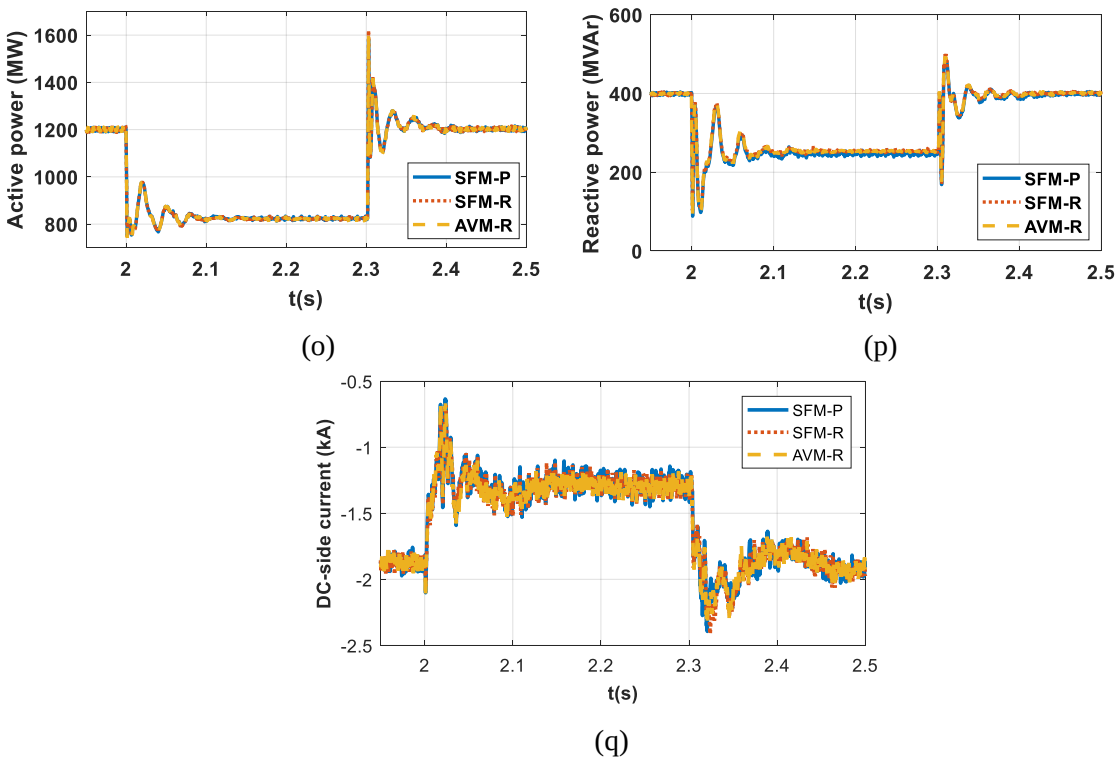

Fig. 5: Simulation waveforms that compare the transient behaviours of 20-cell MMC offline switching function model against that of real-time 20-cell switching function and averaged MMC models during a single-phase-to-ground AC fault

4.2 Three-Phase-to-Ground AC Fault

Fig. 6 displays simulation waveforms for a three-phase-to-ground AC fault. Fig. 6 (a) and (b), (c) and (d), and (e) and (f) show a full-scaled and zoomed simulation waveforms for the three-phase AC voltages at PCC, three-phase AC currents the MMC injects into PCC, and three-phase AC current the MMC injects into low-voltage side of the interfacing transformer (converter side currents). All zoomed waveforms are captured around the instant of fault inception. These waveforms show that the real-time waveforms of the 20-cell switching function and average models are practically indistinguishable, with both exhibit negligible errors relative to that of the offline simulation, particularly in the first few peaks of the AC side currents (grid and converter sides). Similarly, the plots for the upper and lower arm currents displayed in Fig. 6(g) and (h), and (i) and (j) also show small errors appear briefly in the first few peaks of the arm current following AC fault inception, and quickly vanished. The plots for the sums of the upper and lower cell capacitors of the three models are compared in Fig. 6 (k) to (n). Fig. 6 (o) and (p) show the waveforms for all capacitor voltages in one arm (phase A upper arm), with the results of real-time and offline PSCAD switching function models are plotted in the top of each other. These waveforms indicate that the real-time and offline simulations exhibit similar behaviours during steady-state and transients, with extremely small errors of less than 1% appear at the instances of fault inception and clearance. Fig. 6(q), (r) and (w) show that the real-time and offline simulation waveforms for the active and reactive powers and DC link current during Three-phase-to-ground AC fault are similar with extremely small errors around the instants of fault inception and clearance.

Detailed corroboration of the real-time and offline simulation results shown in Fig. 6 confirm the suitability of the presented real-time used defined MMC models (20-cell switching function and averaged) for studying three-phase-to-ground AC faults.

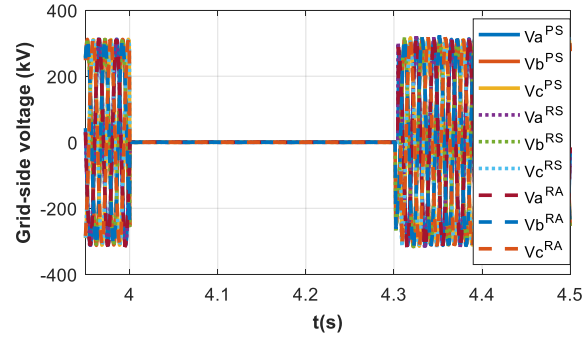

(a)

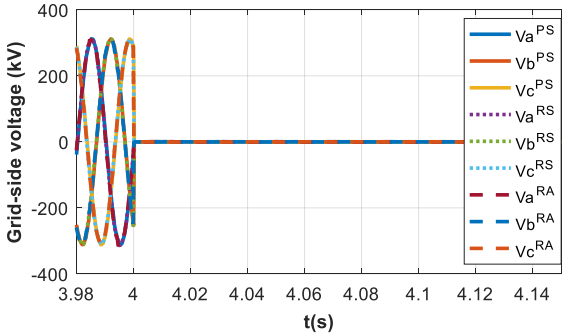

(b)

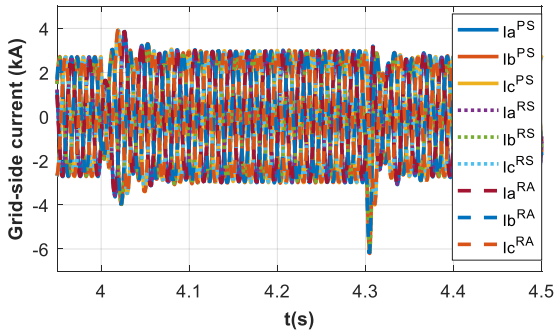

(c)

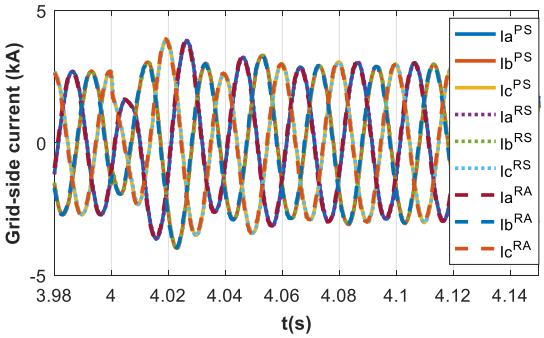

(d)

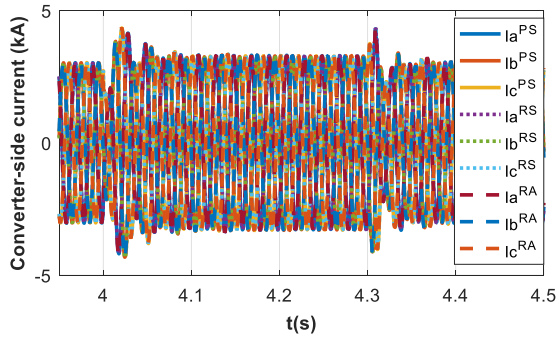

(e)

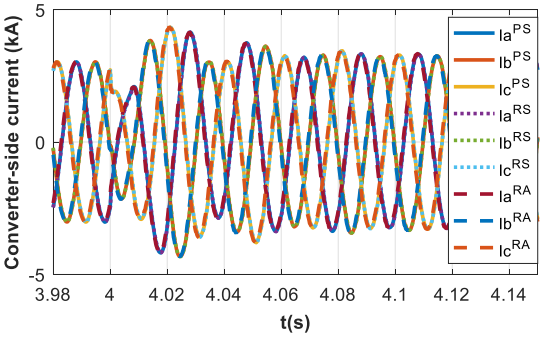

(f)

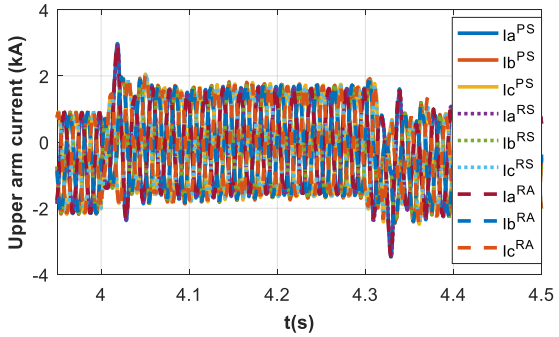

(g)

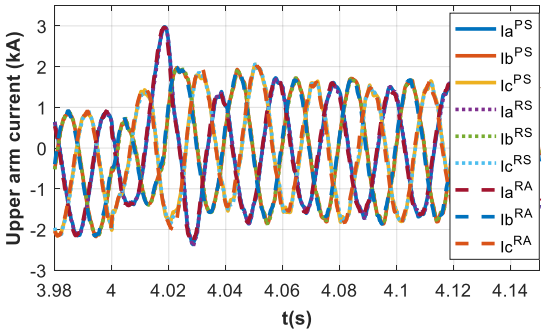

(h)

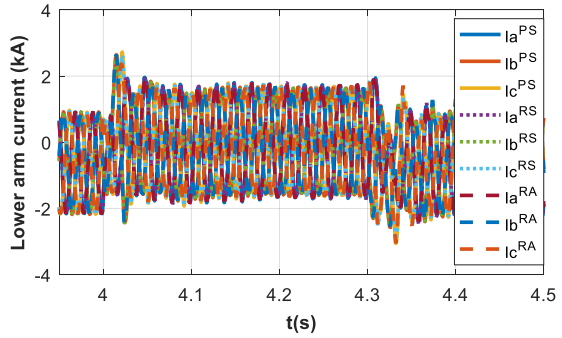
Lower arm current (kA)
t(s)
Ia^PS
Ib^PS
Ic^PS
Ia^RS
Ib^RS
Ic^RS
Ia^RA
Ib^RA
Ic^RA

(i)

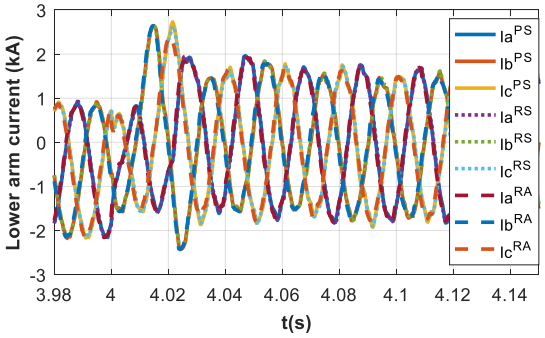
Lower arm current (kA)
t(s)
Ia^PS
Ib^PS
Ic^PS
Ia^RS
Ib^RS
Ic^RS
Ia^RA
Ib^RA
Ic^RA

(j)

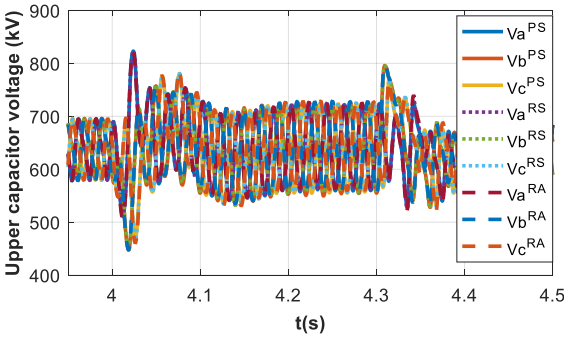
Upper capacitor voltage (kV)
t(s)
Va^PS
Vb^PS
Vc^PS
Va^RS
Vb^RS
Vc^RS
Va^RA
Vb^RA
Vc^RA

(k)

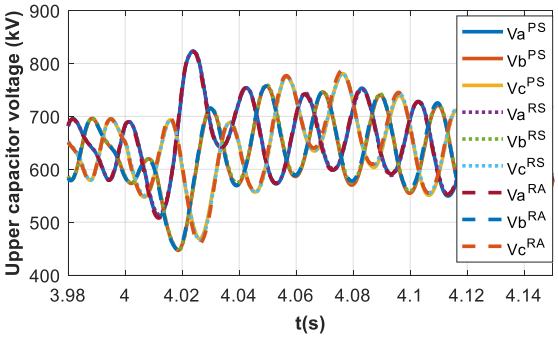
Upper capacitor voltage (kV)
t(s)
Va^PS
Vb^PS
Vc^PS
Va^RS
Vb^RS
Vc^RS
Va^RA
Vb^RA
Vc^RA

(l)

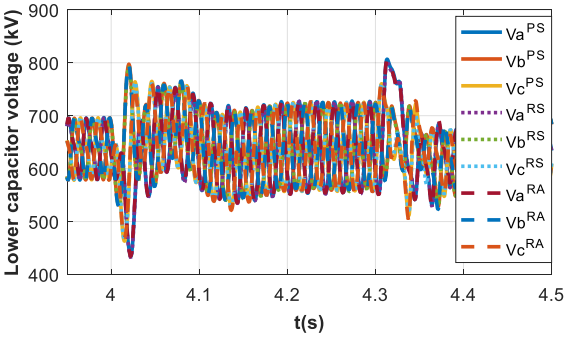
Lower capacitor voltage (kV)
t(s)
Va^PS
Vb^PS
Vc^PS
Va^RS
Vb^RS
Vc^RS
Va^RA
Vb^RA
Vc^RA

(m)

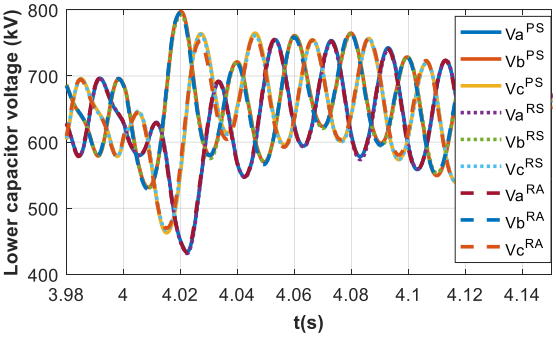
Lower capacitor voltage (kV)
t(s)
Va^PS
Vb^PS
Vc^PS
Va^RS
Vb^RS
Vc^RS
Va^RA
Vb^RA
Vc^RA

(n)

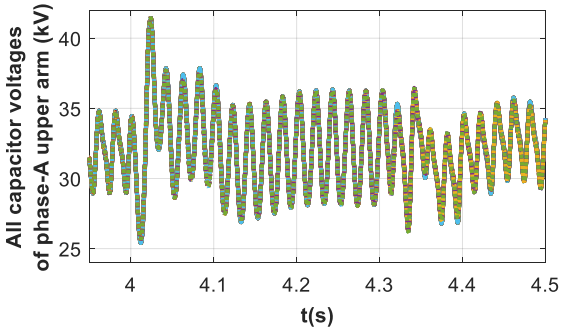
All capacitor voltages of phase-A upper arm (kV)
t(s)

(o)

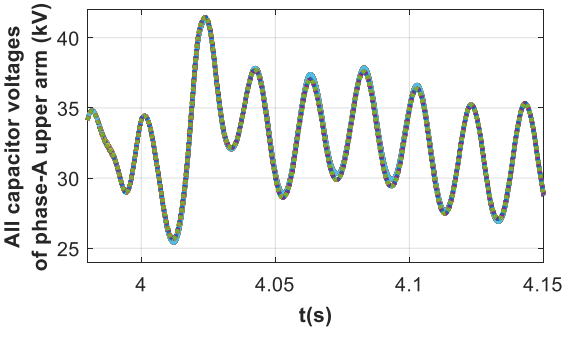
All capacitor voltages of phase-A upper arm (kV)
t(s)

(p)

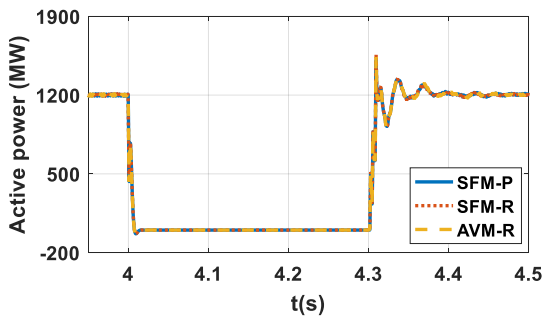

(q)

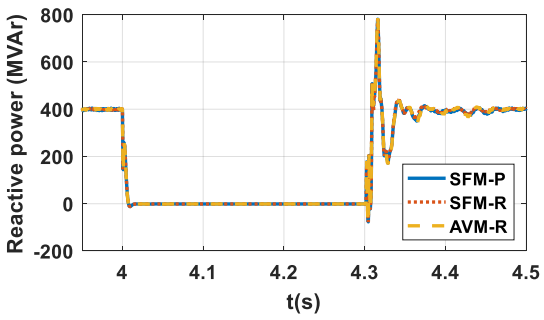

(r)

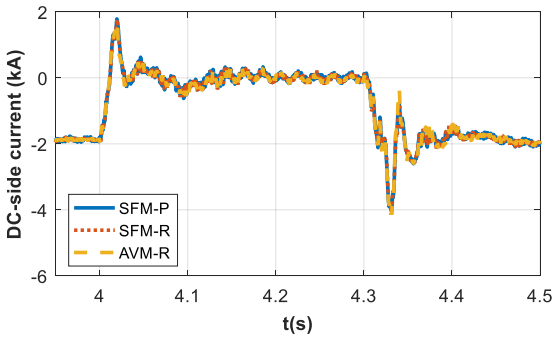

(s)

Fig. 6: Simulation waveforms that compare the transient behaviours of 20-cell MMC offline switching function model against that of the real-time 20-cell switching function and averaged MMC models during a three-phase-to-ground AC fault

4.3 Phase-to-Phase AC Fault

Fig. 7 presents simulation waveforms for a phase-to-phase AC fault at PCC. Fig. 7(a) and (b), (c) and (d), and (e) and (f) show simulation waveforms for the three-phase AC voltages at PCC, three-phase AC currents the MMC injects into PCC, and three-phase AC currents the MMC injects into low-voltage side of the interfacing transformer (converter side currents), including expanded snapshots around the instant of fault inception. These waveforms show that the real-time waveforms of the 20-cell switching function and average models are similar, with both real-time averaged and switching function models exhibit negligible errors relative to the 20-cell switching function offline simulation, particularly, including in the first few peaks of the AC side currents (grid and converter sides). Likewise, the plots for the upper and lower arm currents displayed in Fig. 7(g) and (h), and (i) and (j) show small errors, which appear briefly, in the first few peaks of the arm current, following the AC fault inception and quickly subsided. The plots for the sums of the upper and lower cell capacitors of the three models being compared in Fig. 7(k) to (m) indicate that the real-time and offline simulations exhibit similar behaviours during steady-state and transients, with small errors of less than 1% in the cell capacitor voltages, arm currents, three-phase output currents and dc link current. Fig. 7(o), (p) and (q) show that the real-time and offline simulation waveforms for the active and reactive powers and DC link current during phase-to-phase AC fault are similar, with small and diminished errors observed around the instants of fault inception and clearance. The reactive power errors

shown in Fig. 8(q) between offline and real-time simulation results for reactive powers are due to the same reason explained in section 4.1 (Single-Phase-to Ground AC Fault case).

One-to-one validation of the real-time and offline simulation results shown in Fig. 8 confirm the suitability of the presented real-time used defined MMC models (20-cell switching function and averaged) for studying phase-to-phase AC faults.

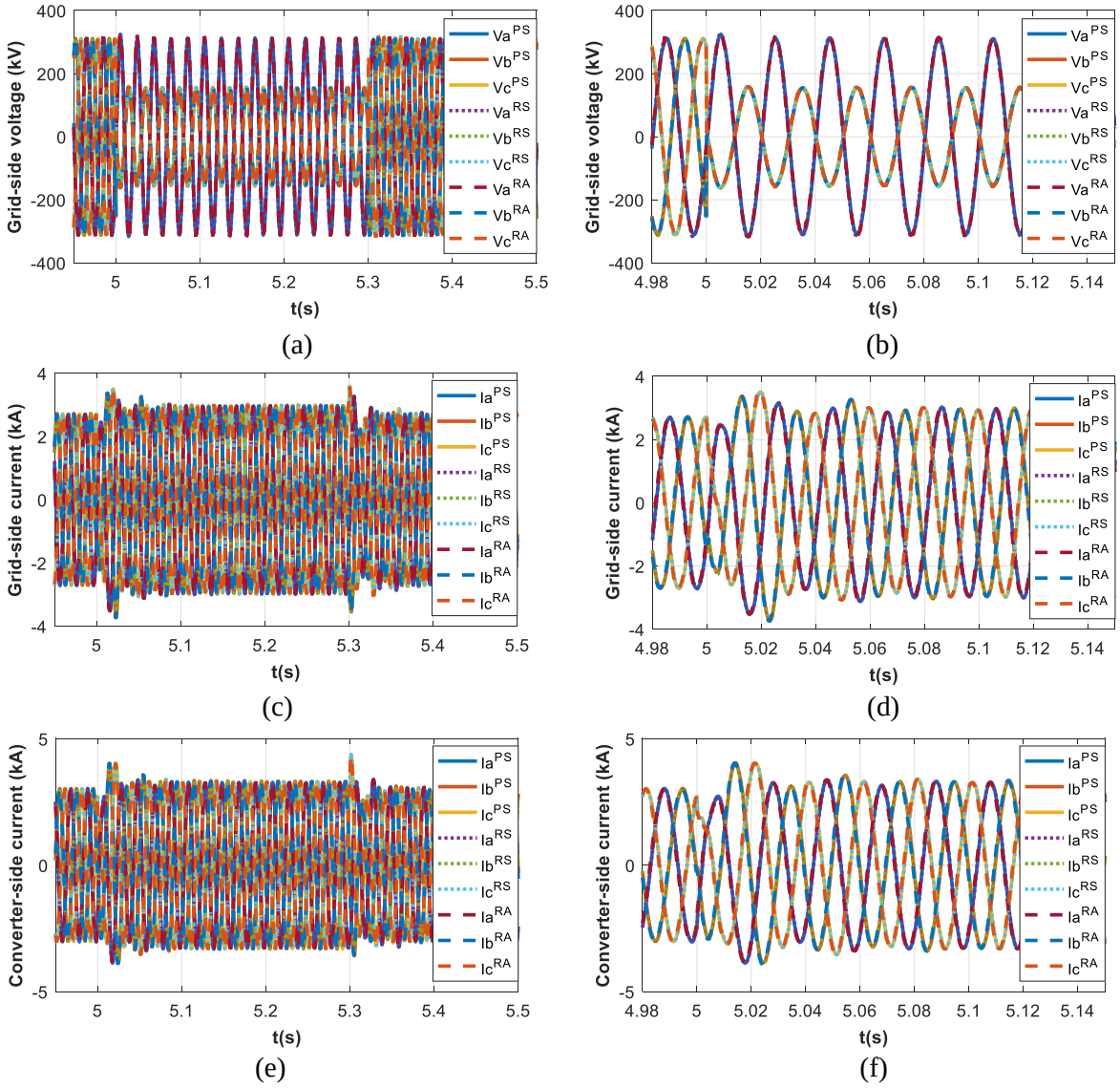

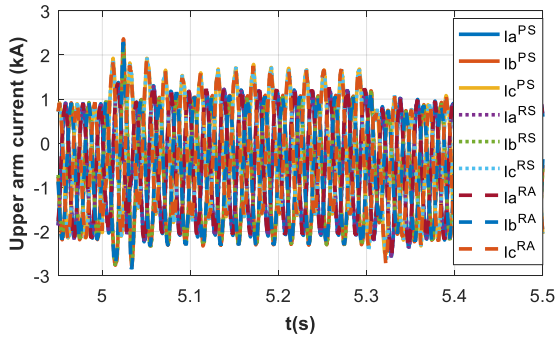
Upper arm current (kA)
t(s)
Ia^PS
Ib^PS
Ic^PS
Ia^RS
Ib^RS
Ic^RS
Ia^RA
Ib^RA
Ic^RA

(g)

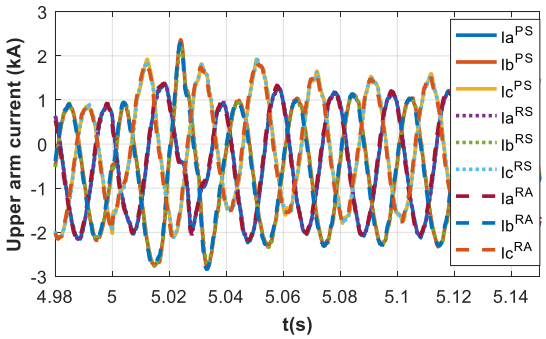
Upper arm current (kA)
t(s)
Ia^PS
Ib^PS
Ic^PS
Ia^RS
Ib^RS
Ic^RS
Ia^RA
Ib^RA
Ic^RA

(h)

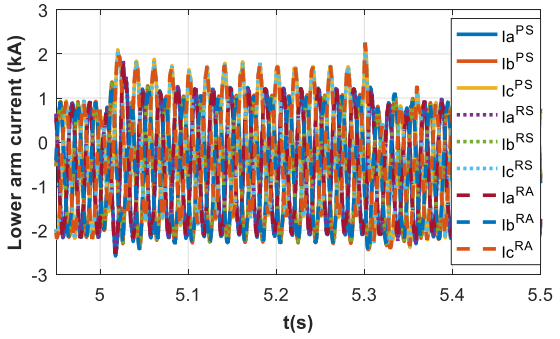
Lower arm current (kA)
t(s)
Ia^PS
Ib^PS
Ic^PS
Ia^RS
Ib^RS
Ic^RS
Ia^RA
Ib^RA
Ic^RA

(i)

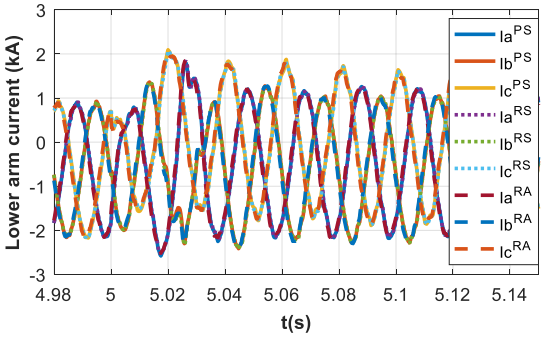
Lower arm current (kA)
t(s)
Ia^PS
Ib^PS
Ic^PS
Ia^RS
Ib^RS
Ic^RS
Ia^RA
Ib^RA
Ic^RA

(j)

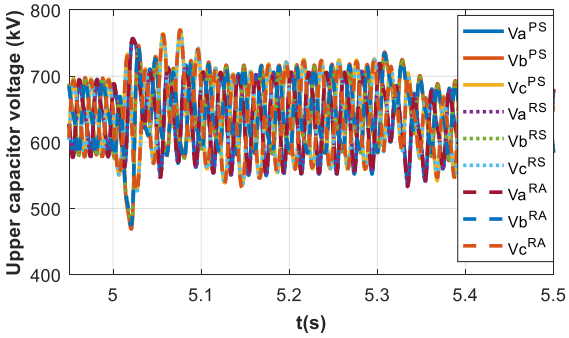
Upper capacitor voltage (kV)
t(s)
Va^PS
Vb^PS
Vc^PS
Va^RS
Vb^RS
Vc^RS
Va^RA
Vb^RA
Vc^RA

(k)

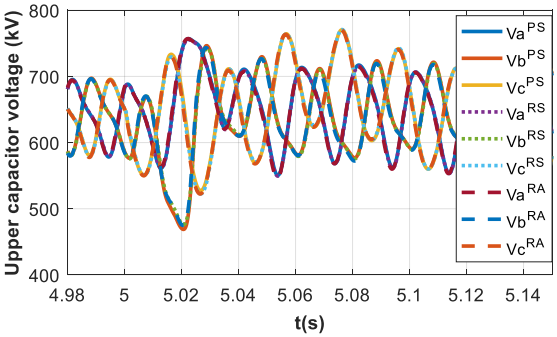
Upper capacitor voltage (kV)
t(s)
Va^PS
Vb^PS
Vc^PS
Va^RS
Vb^RS
Vc^RS
Va^RA
Vb^RA
Vc^RA

(l)

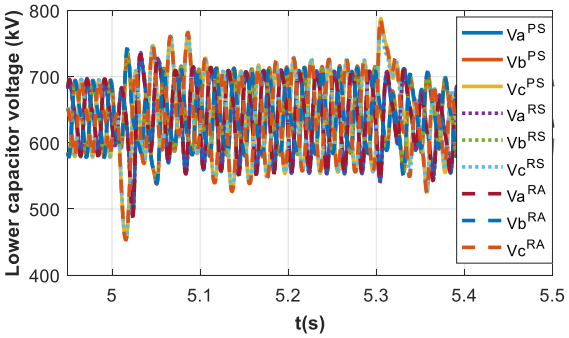
Lower capacitor voltage (kV)
t(s)
Va^PS
Vb^PS
Vc^PS
Va^RS
Vb^RS
Vc^RS
Va^RA
Vb^RA
Vc^RA

(m)

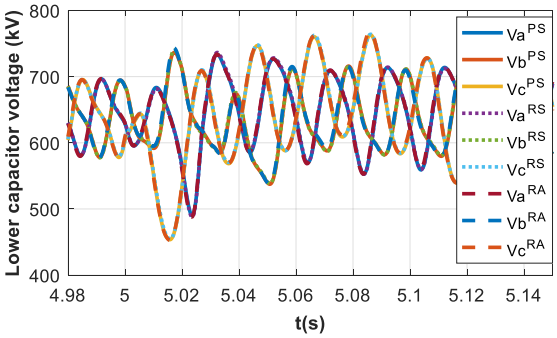
Lower capacitor voltage (kV)
t(s)
Va^PS
Vb^PS
Vc^PS
Va^RS
Vb^RS
Vc^RS
Va^RA
Vb^RA
Vc^RA

(n)

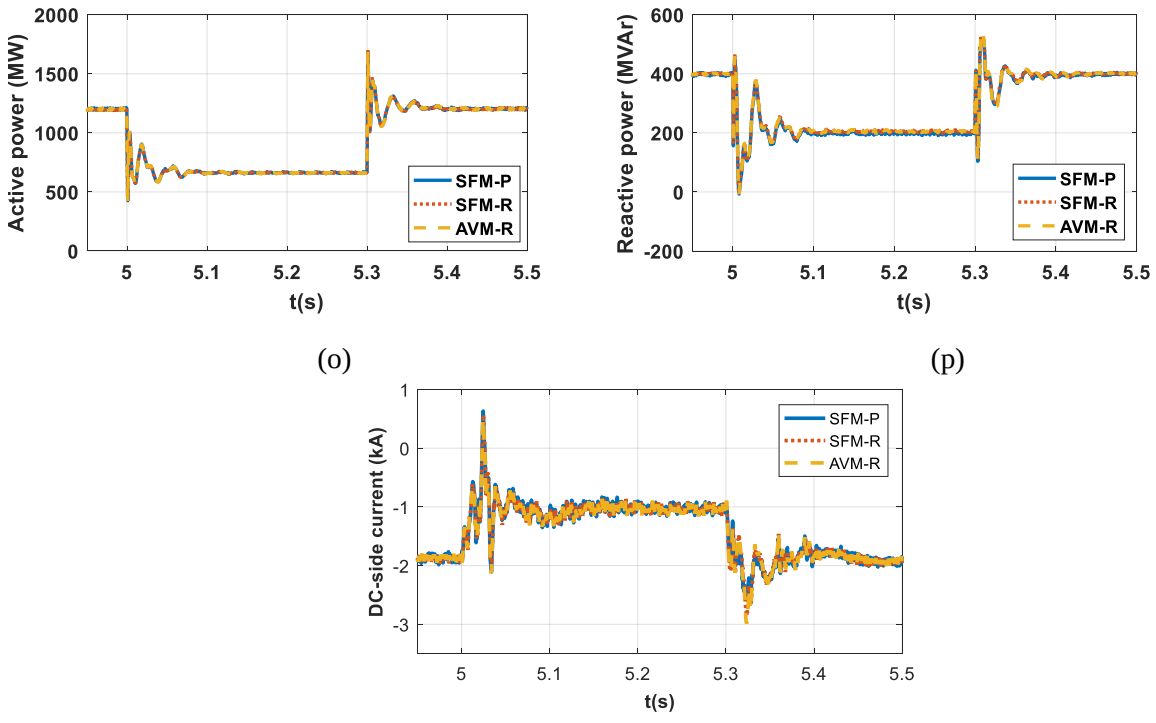

Fig. 7: Simulation waveforms that compare the transient behaviours of 20-cell MMC offline switching function model against that of real-time 20-cell switching function and averaged MMC models during a phase-to-phase-to AC fault

4.4 Pole-to-Pole DC Short Circuit Fault

Fig. 8 presents simulation waveforms for a solid pole-to-pole DC fault right at MMC DC terminals. Fig. 8 (a) and (b), (c) and (d), and (e) and (f) show simulation waveforms for the three-phase AC voltages at PCC, three-phase AC currents the MMC injects into PCC, and three-phase AC currents the MMC injects into low-voltage side of the interfacing transformer (converter side currents), including the expanded snapshots around the instant of fault inception. These traces show that all the real-time and offline simulations waveforms are identical (real-time simulation waveforms of the 20-cell switching function and average models superimposed on that of the 20-cell offline PSCAD waveforms). Also, the upper and lower arm currents real-time and offline simulation waveforms displayed in Fig. 8 (g) and (h), and (i) and (j) do not exhibit any visible errors in steady-state and during DC fault. The real-time and offline simulation plots for the sums of the upper and lower arm cell capacitors of the three models are compared in Fig. 8 (k) to (m). Fig. 8 (o) and (p) show simulation waveforms of all capacitor voltages in one arm (phase A upper arm) and their snapshots zoomed around fault inception, with the real-time waveforms (RTDS switching function model) superimposed on the equivalent offline simulation waveforms (PSCAD switching function model). These waveforms indicate that the real-time and offline simulations exhibit identical behaviours during steady-state and fault periods. Fig. 8 (q), (r), (s) and (t) show that the real-time and offline simulation waveforms for the active and reactive powers, and DC link current and voltage during DC short circuit are similar, with small difference in the active powers during fault period. The differences obseved in the active

power during dc fault is due to small differences in the total resistance in the fault current path, which come implementation of the parts that mimic the blocking of phsysical MMC (recall that the two platforms, PSCAD and RSCAD have different implementation of the IGBTs and diodes). These differences are excerbated during DC short circuit fault by the signifcant increase in the magnitude of the fault currents relative to rated currents. The differences in the resistances of conduction path between the two platforms lead to the rated active power (1200MW) to be achieved with slightly different, i_d.

Results of detailed validation displayed in Fig. 8 confirm the appropriateness of the presented real-time user-defined MMC models (20-cell switching function and averaged) for studying pole-to-pole DC short circuit faults.

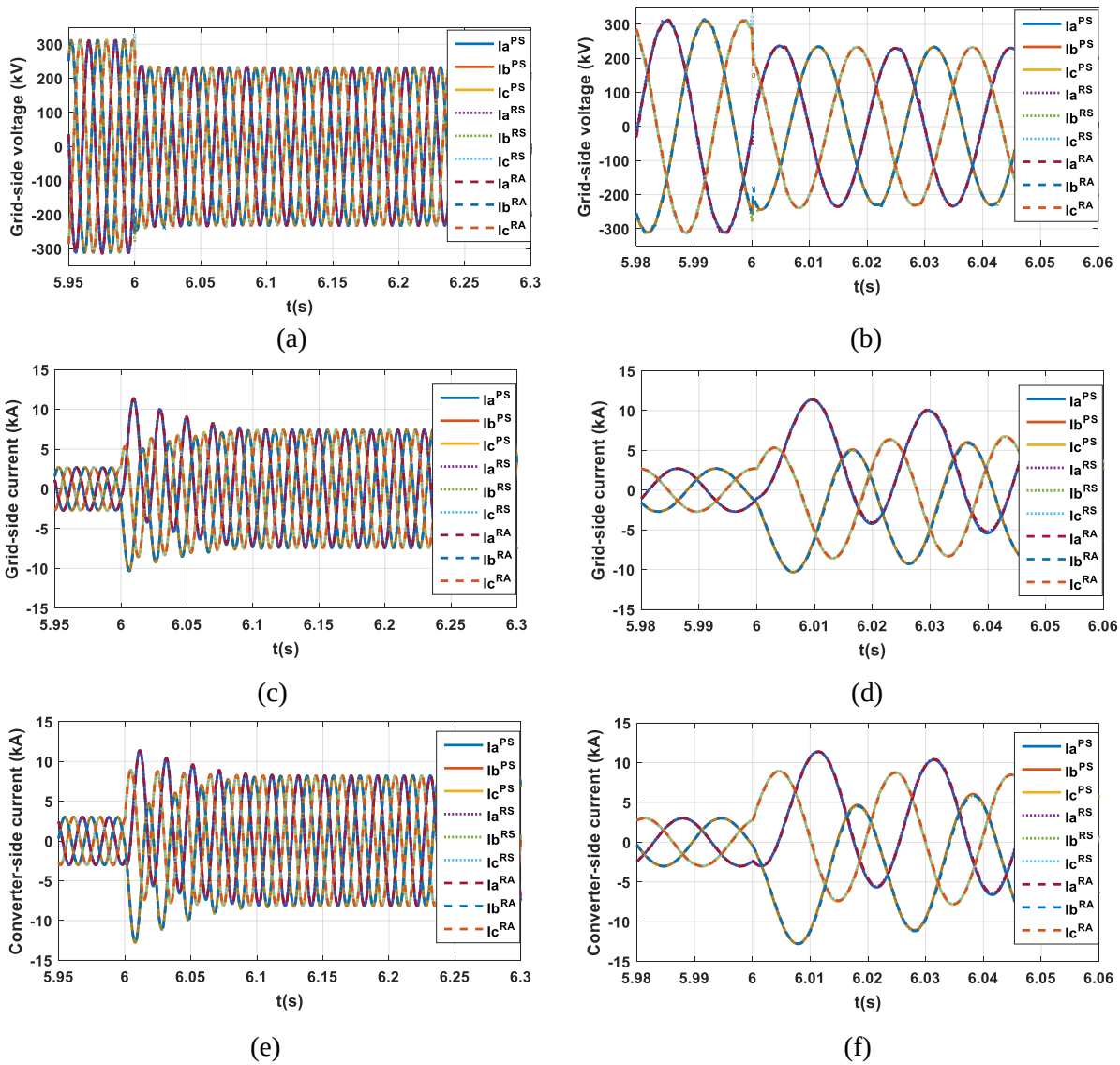

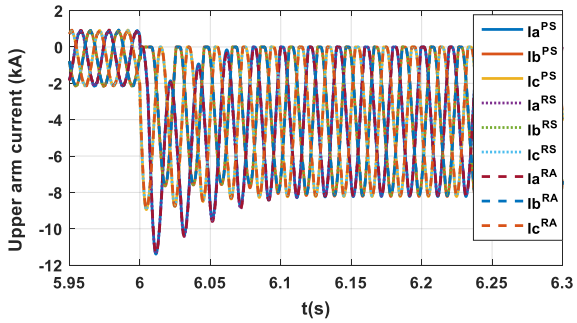
Upper arm current (kA)
t(s)
Ia^PS
Ib^PS
Ic^PS
Ia^RS
Ib^RS
Ic^RS
Ia^RA
Ib^RA
Ic^RA

(g)

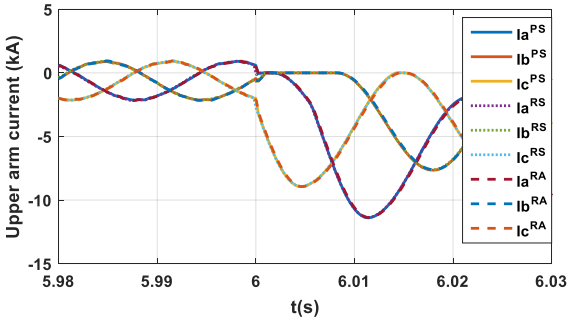
Upper arm current (kA)
t(s)
Ia^PS
Ib^PS
Ic^PS
Ia^RS
Ib^RS
Ic^RS
Ia^RA
Ib^RA
Ic^RA

(h)

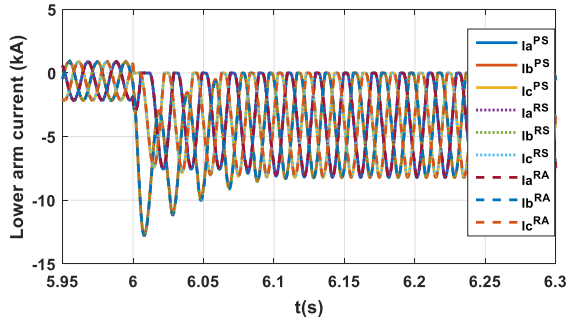
Lower arm current (kA)
t(s)
Ia^PS
Ib^PS
Ic^PS
Ia^RS
Ib^RS
Ic^RS
Ia^RA
Ib^RA
Ic^RA

(i)

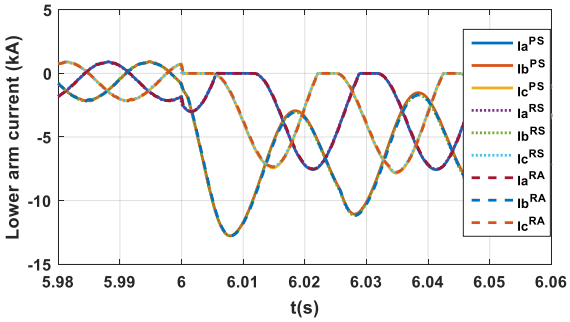
Lower arm current (kA)
t(s)
Ia^PS
Ib^PS
Ic^PS
Ia^RS
Ib^RS
Ic^RS
Ia^RA
Ib^RA
Ic^RA

(j)

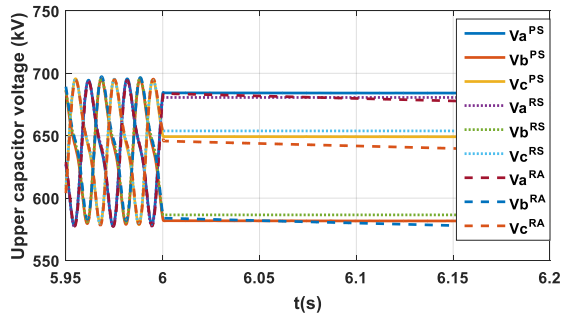
Upper capacitor voltage (kV)
t(s)
Va^PS
Vb^PS
Vc^PS
Va^RS
Vb^RS
Vc^RS
Va^RA
Vb^RA
Vc^RA

(k)

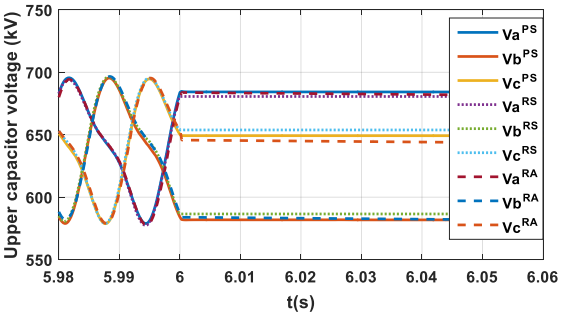
Upper capacitor voltage (kV)
t(s)
Va^PS
Vb^PS
Vc^PS
Va^RS
Vb^RS
Vc^RS
Va^RA
Vb^RA
Vc^RA

(l)

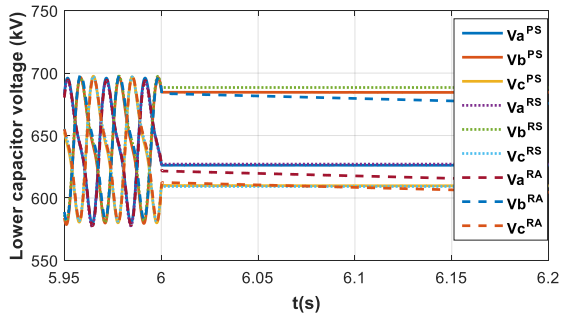
Lower capacitor voltage (kV)
t(s)
Va^PS
Vb^PS
Vc^PS
Va^RS
Vb^RS
Vc^RS
Va^RA
Vb^RA
Vc^RA

(m)

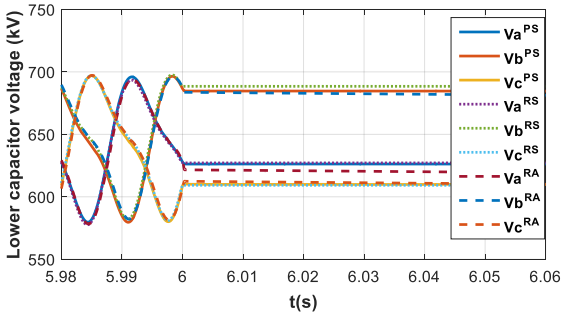
Lower capacitor voltage (kV)
t(s)
Va^PS
Vb^PS
Vc^PS
Va^RS
Vb^RS
Vc^RS
Va^RA
Vb^RA
Vc^RA

(n)

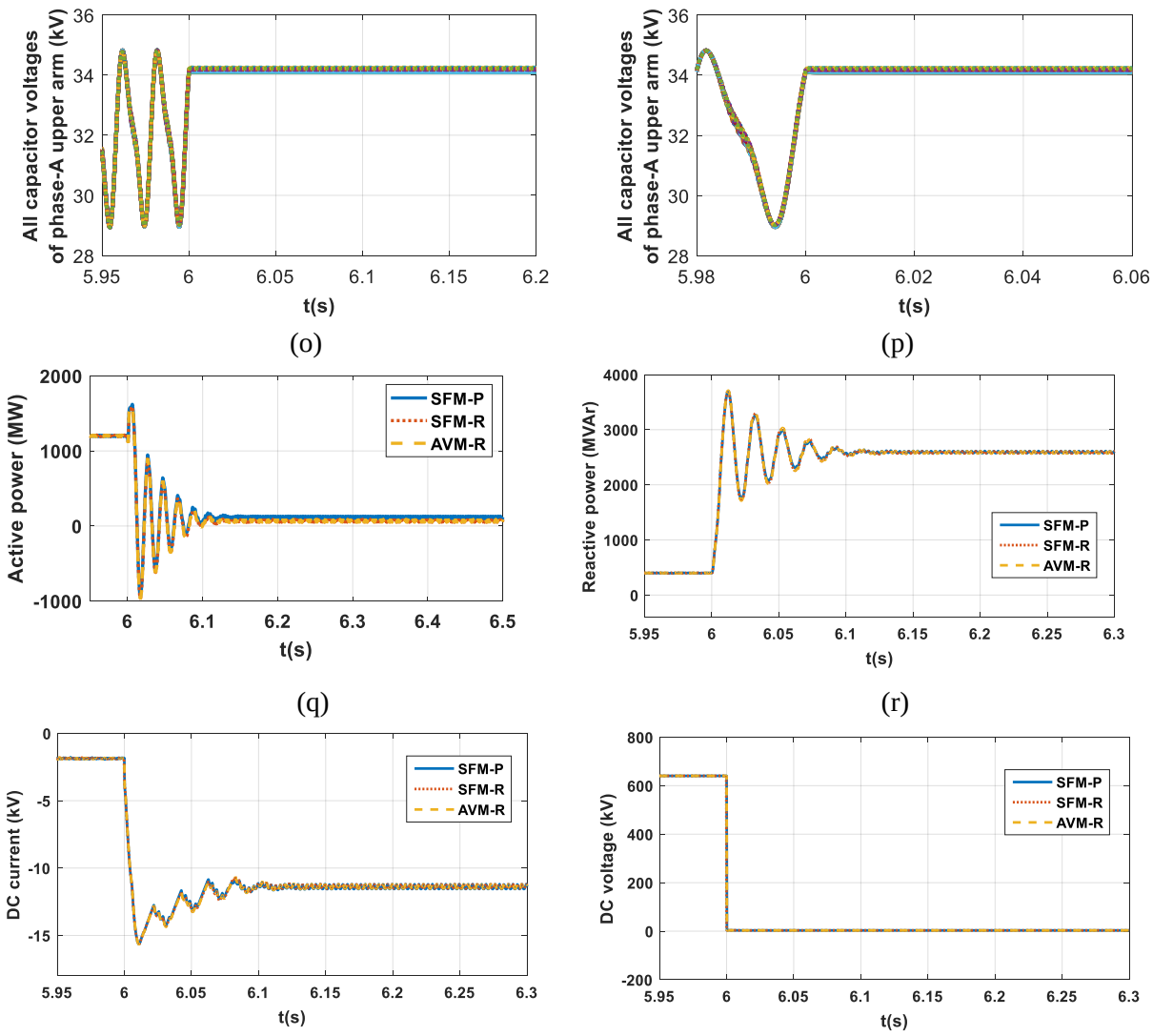

Fig. 8: Simulation waveforms that compare the transient behaviours of the developed MMC (SF vs Avg) models during DC short circuit fault (SCR=10)

4.5 Pole-to-ground DC Fault

The results during the pole-to-ground DC fault are shown in Fig. 9. The connection between DC side and the converter is implemented by 50km pi-sections. Fig. 9 presents simulation waveforms when a negative DC cable (pole) of a symmetrical monopole is subjected to a pole-to-ground DC fault right at the DC terminals of the MMC.

Fig. 9 (a) and (b) show offline and real-time simulation waveforms for the DC voltages of the positive and negative DC cables and DC link currents, with DC voltage waveforms exhibit not visible differences, while DC currents show minor differences. Fig. 9 (c) presents the traces for the three-phase AC voltage waveforms of the offline and real-time simulations that the MMC presents to the low-voltage windings of

the interfacing transformer, and it can be observed that a DC offset amounts to half of the DC link voltage appears with the inception of the pole-to-ground DC fault as expected. In contrast, the plots for the three-phase AC currents that the MMC presents to low-voltage windings of the interfacing transformer remain unaffected by the pole-to-ground DC fault, Fig. 9 (d). Offline and real-time simulation waveforms for the upper and lower arm currents and sums of the cell capacitor voltages displayed in Fig. 9 (e) and (f), and (g) and (h) do not reveal significant errors during steady-state and pole-to-ground DC fault.

Based on the results in Fig. 9, it can be concluded the validity of the presented real-time user-defined MMC models (20-cell switching function and averaged) for studying pole-to-ground DC faults is confirmed.

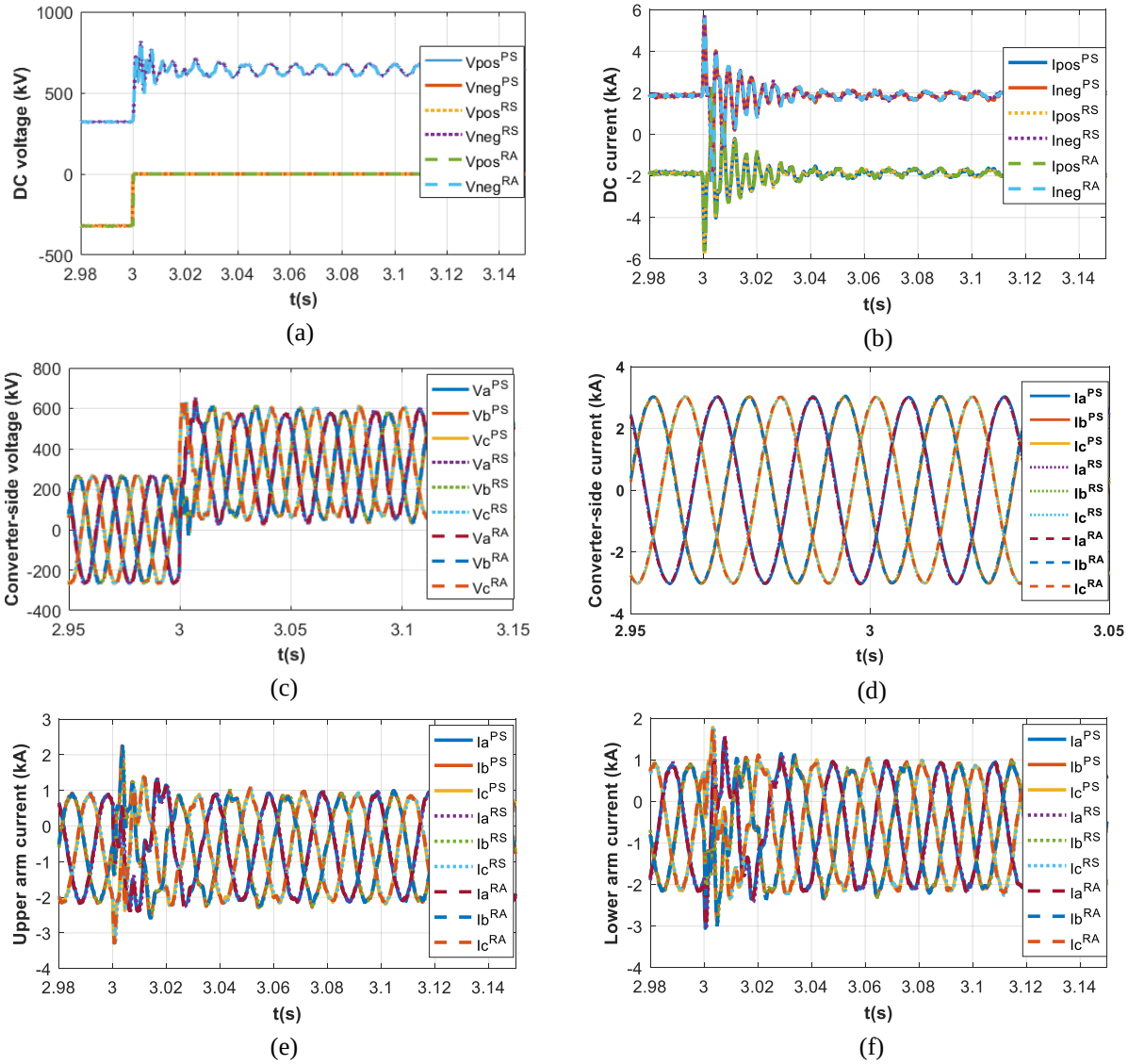

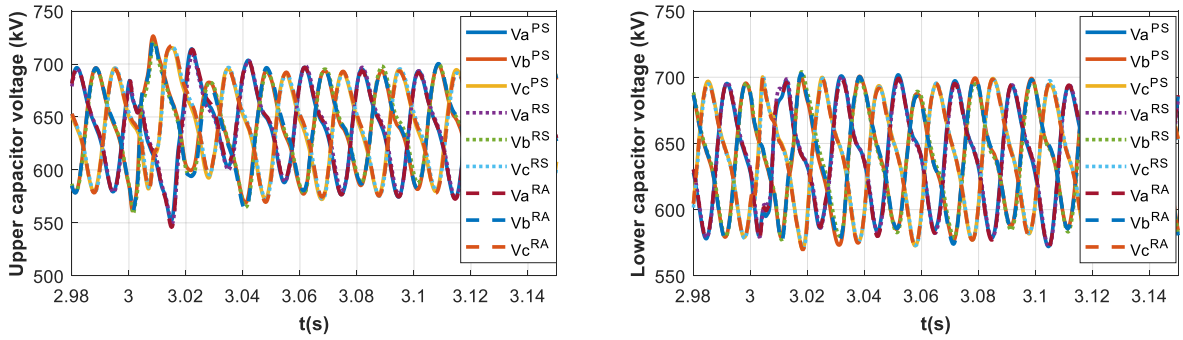

(g) (h)

Fig. 9: Simulation waveforms that illustrate the transient response of the switching function MMC model to a pole-to-ground DC fault

4.6 **Three-Phase-to-Ground AC Fault in Weak Grid**

Fig. 10 presents simulation waveforms for a three-phase-to-ground AC fault when the MMC operates in a weak AC grid with SCR=3 and receiving 400MVAr from AC grid.

Fig. 10 (a) and (b), (c) and (d), and (e) and (f) show a full-scaled and zoomed simulation waveforms for the three-phase AC voltages at PCC, three-phase AC currents the MMC injects into PCC, and three-phase AC current the MMC injects into low-voltage side of the interfacing transformer (converter side currents). All zoomed waveforms are captured around the instant of fault inception. These waveforms show that the real-time waveforms of the 20-cell switching function and average models are practically indistinguishable, with both exhibit similar results as the offline simulation. Similarly, the plots for the upper and lower arm currents displayed in Fig. 10 (g) and (h), and (i) and (j) also show practically identical results during steady-state and at AC fault inception. The plots for the sums of the upper and lower cell capacitors of the three models being compared in (k) to (m) indicate that the real-time and offline simulations exhibit similar behaviours during steady-state and transients, with extremely small errors of much less than 1% appear at the instances of fault inception and clearance. Fig. 10 (o), (p) and (q) show that the real-time and offline simulation waveforms for the active and reactive powers and DC link current during three-phase-to-ground AC fault are similar with extremely small errors around the instants of fault inception and clearance.

Detailed corroboration of the real-time and offline simulation results shown in Fig. 6 and Fig. 10 confirm the suitability of the presented real-time used defined MMC models (20-cell switching function and averaged) for studying three-phase-to-ground AC faults in weak AC systems.

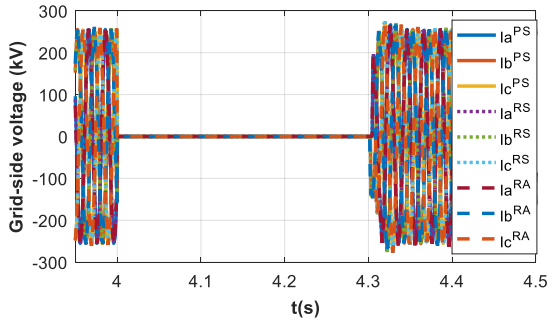
Grid-side voltage (kV)
t(s)
Ia^{PS}
Ib^{PS}
Ic^{PS}
Ia^{RS}
Ib^{RS}
Ic^{RS}
Ia^{RA}
Ib^{RA}
Ic^{RA}

(a)

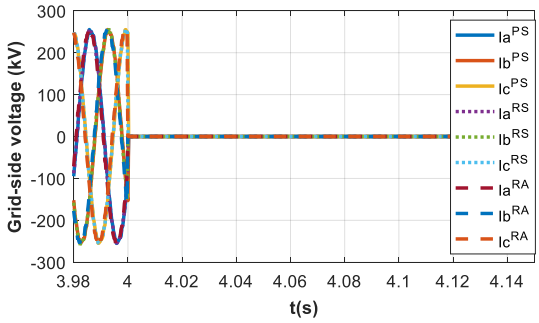
Grid-side voltage (kV)
t(s)
Ia^{PS}
Ib^{PS}
Ic^{PS}
Ia^{RS}
Ib^{RS}
Ic^{RS}
Ia^{RA}
Ib^{RA}
Ic^{RA}

(b)

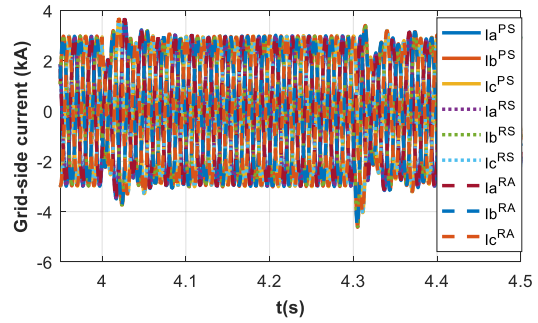
Grid-side current (kA)
t(s)
Ia^{PS}
Ib^{PS}
Ic^{PS}
Ia^{RS}
Ib^{RS}
Ic^{RS}
Ia^{RA}
Ib^{RA}
Ic^{RA}

(c)

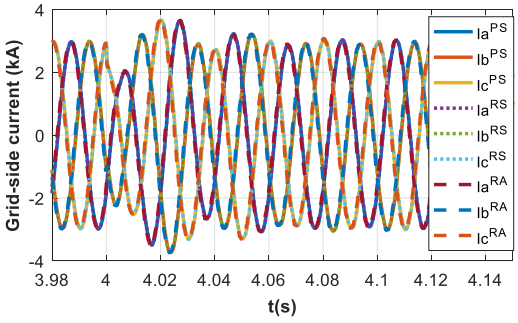
Grid-side current (kA)
t(s)
Ia^{PS}
Ib^{PS}
Ic^{PS}
Ia^{RS}
Ib^{RS}
Ic^{RS}
Ia^{RA}
Ib^{RA}
Ic^{RA}

(d)

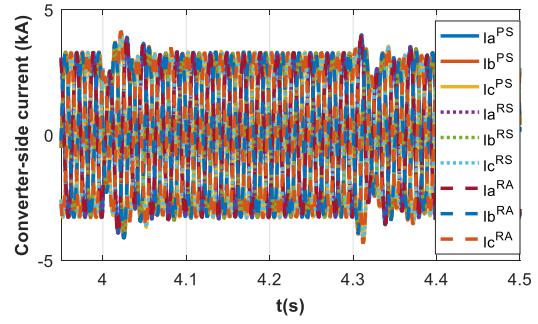
Converter-side current (kA)
t(s)
Ia^{PS}
Ib^{PS}
Ic^{PS}
Ia^{RS}
Ib^{RS}
Ic^{RS}
Ia^{RA}
Ib^{RA}
Ic^{RA}

(e)

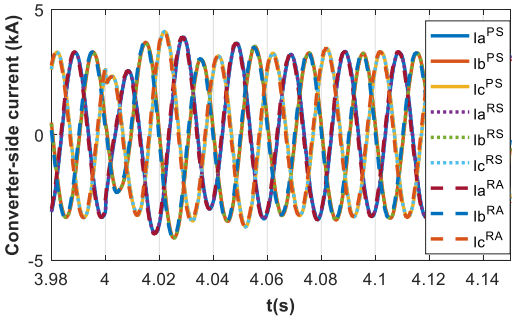
Converter-side current (kA)
t(s)
Ia^{PS}
Ib^{PS}
Ic^{PS}
Ia^{RS}
Ib^{RS}
Ic^{RS}
Ia^{RA}
Ib^{RA}
Ic^{RA}

(f)

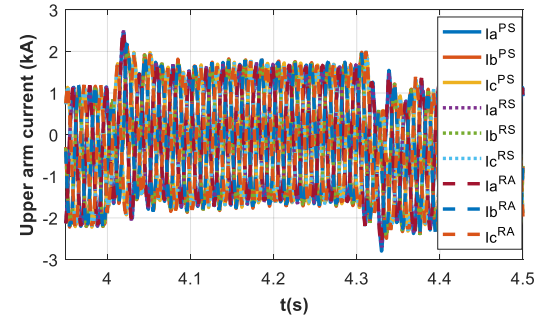
Upper arm current (kA)
t(s)
Ia^{PS}
Ib^{PS}
Ic^{PS}
Ia^{RS}
Ib^{RS}
Ic^{RS}
Ia^{RA}
Ib^{RA}
Ic^{RA}

(g)

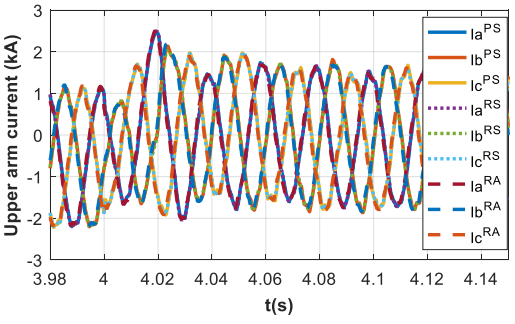
Upper arm current (kA)
t(s)
Ia^{PS}
Ib^{PS}
Ic^{PS}
Ia^{RS}
Ib^{RS}
Ic^{RS}
Ia^{RA}
Ib^{RA}
Ic^{RA}

(h)

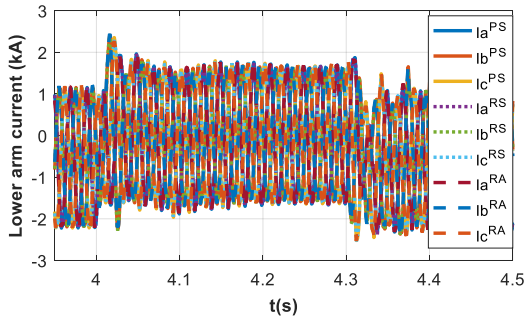
Lower arm current (kA)
t(s)
Ia^PS
Ib^PS
Ic^PS
Ia^RS
Ib^RS
Ic^RS
Ia^RA
Ib^RA
Ic^RA

(i)

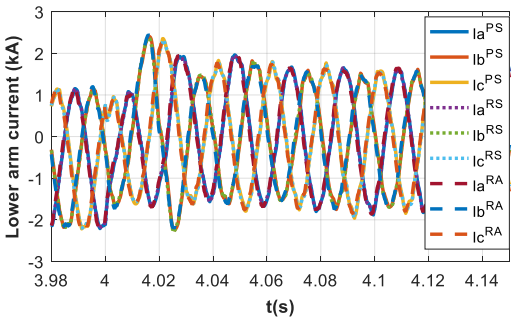
Lower arm current (kA)
t(s)
Ia^PS
Ib^PS
Ic^PS
Ia^RS
Ib^RS
Ic^RS
Ia^RA
Ib^RA
Ic^RA

(j)

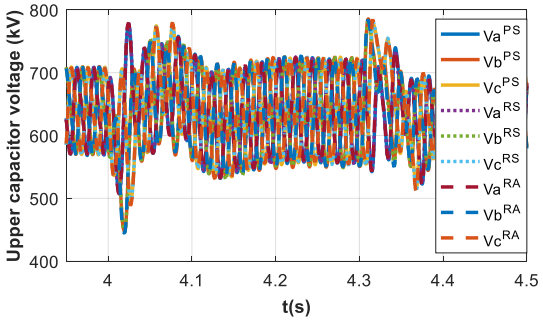
Upper capacitor voltage (kV)
t(s)
Va^PS
Vb^PS
Vc^PS
Va^RS
Vb^RS
Vc^RS
Va^RA
Vb^RA
Vc^RA

(k)

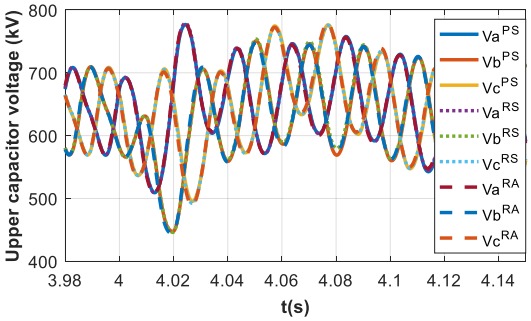
Upper capacitor voltage (kV)
t(s)
Va^PS
Vb^PS
Vc^PS
Va^RS
Vb^RS
Vc^RS
Va^RA
Vb^RA
Vc^RA

(l)

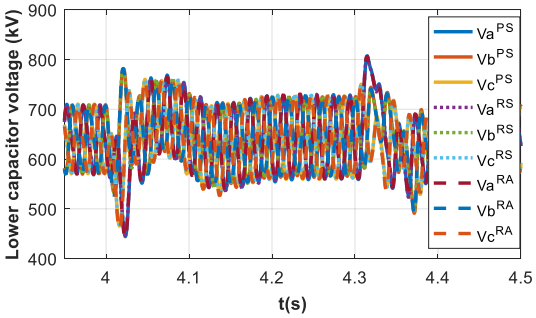
Lower capacitor voltage (kV)
t(s)
Va^PS
Vb^PS
Vc^PS
Va^RS
Vb^RS
Vc^RS
Va^RA
Vb^RA
Vc^RA

(m)

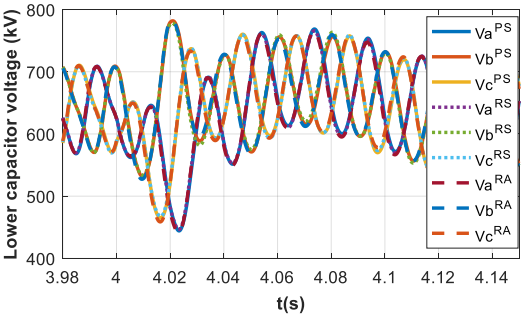
Lower capacitor voltage (kV)
t(s)
Va^PS
Vb^PS
Vc^PS
Va^RS
Vb^RS
Vc^RS
Va^RA
Vb^RA
Vc^RA

(n)

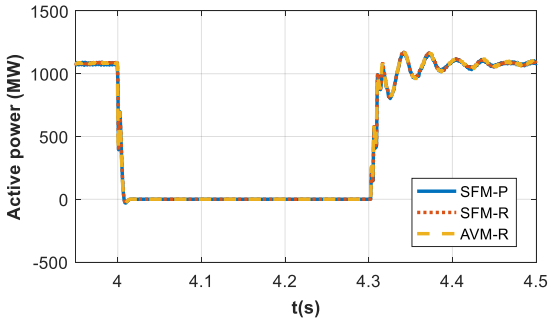
Active power (MW)
t(s)
SFM-P
SFM-R
AVM-R

(o)

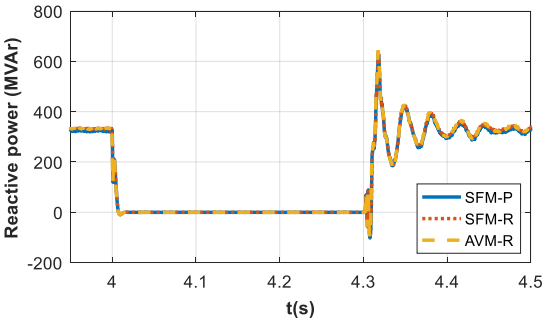
Reactive power (MVAr)
t(s)
SFM-P
SFM-R
AVM-R

(p)

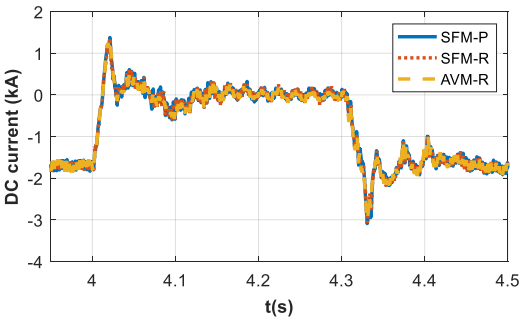

(q)

Fig. 10: Simulation waveforms that compare the transient behaviours of 20-cell MMC offline switching function model against that of the real-time 20-cell switching function and averaged MMC models during a three-phase-to-ground AC fault that occurs in weak AC grid with SCR=3

5 Real-Time Benchmarking of the user defined averaged MMC model

Since detailed validations presented in Section 4 prove that the developed offline and real-time MMC models (switching function and averaged) produce reasonably identical results during normal operation and fault conditions, this section selects a real-time user-defined averaged MMC model for further benchmarking against the MMC5 available in the RTDS library. Both models use the same controllers developed by University of Strathclyde and used in the validation presented in Section 4. The pre-fault, fault and post-fault operating conditions in this benchmarking remain the same as that in Section 4, and only results for symmetrical three-phase-to-ground AC fault will be presented and discussed in this section (worst-case scenario).

Fig. 11 displays selected simulation waveforms that aim to show different dynamics that may occur in the MMC during three-phase-to-ground AC fault. Throughout this section the results of the user defined averaged HB-MMC model are signified by dot lines and supplemented by affix ‘AVG’, and superimposed on that of the benchmark model (MMC5) which are signified by solid lines and supplemented by affix ‘MMC5’.

Fig. 11(a) and (b) show three-phase currents measured at converter side and their snapshots, zoomed around the instant of fault inception. The current waveforms in Fig. 11(a) and (b) confirm that the user-defined averaged HB-MMC model presented in this report and validated against other user-defined offline and real-time HB-MMC models in section 4 produces results that well-matched with that of the MMC5, including during normal operation and three-phase fault as indicated by the sections of current waveforms that capture the behaviour prior the fault inception and during fault period.

Fig. 11(c) and (d) display samples of the arm currents, particularly, phase ‘A’ upper and lower arm currents. These arm current waveforms show that the real-time user-defined averaged HB-MMC model and benchmark HB-MMC model ‘MMC5’ exhibit identical behaviours during steady-state and three-phase AC fault, including during the transition between the two states.

Fig. 11(e) and (f) display samples of the sums of the capacitor voltages in the arms of the HB-MMC, particularly, phase ‘A’ upper and lower arms. The plots in Fig. 11(e) and (f) confirm that the real-time user-defined averaged HB-MMC model and benchmark HB-MMC model ‘MMC5’ have the same dynamic

behaviour during steady-state and three-phase AC fault, including during the transition between the two states (from initial steady-state to new temporary steady-state during fault period).

From the full agreement of the simulation waveforms displayed in Fig. 11(a) through (f), it can be concluded that the real-time user-defined averaged HB-MMC model against benchmark RTDS MMC5, real-time user-defined switching function, and a number of offline HB-MMC models in Section 4 and previous report confirm its validity, and validity of the other models presented in this report and previous report.

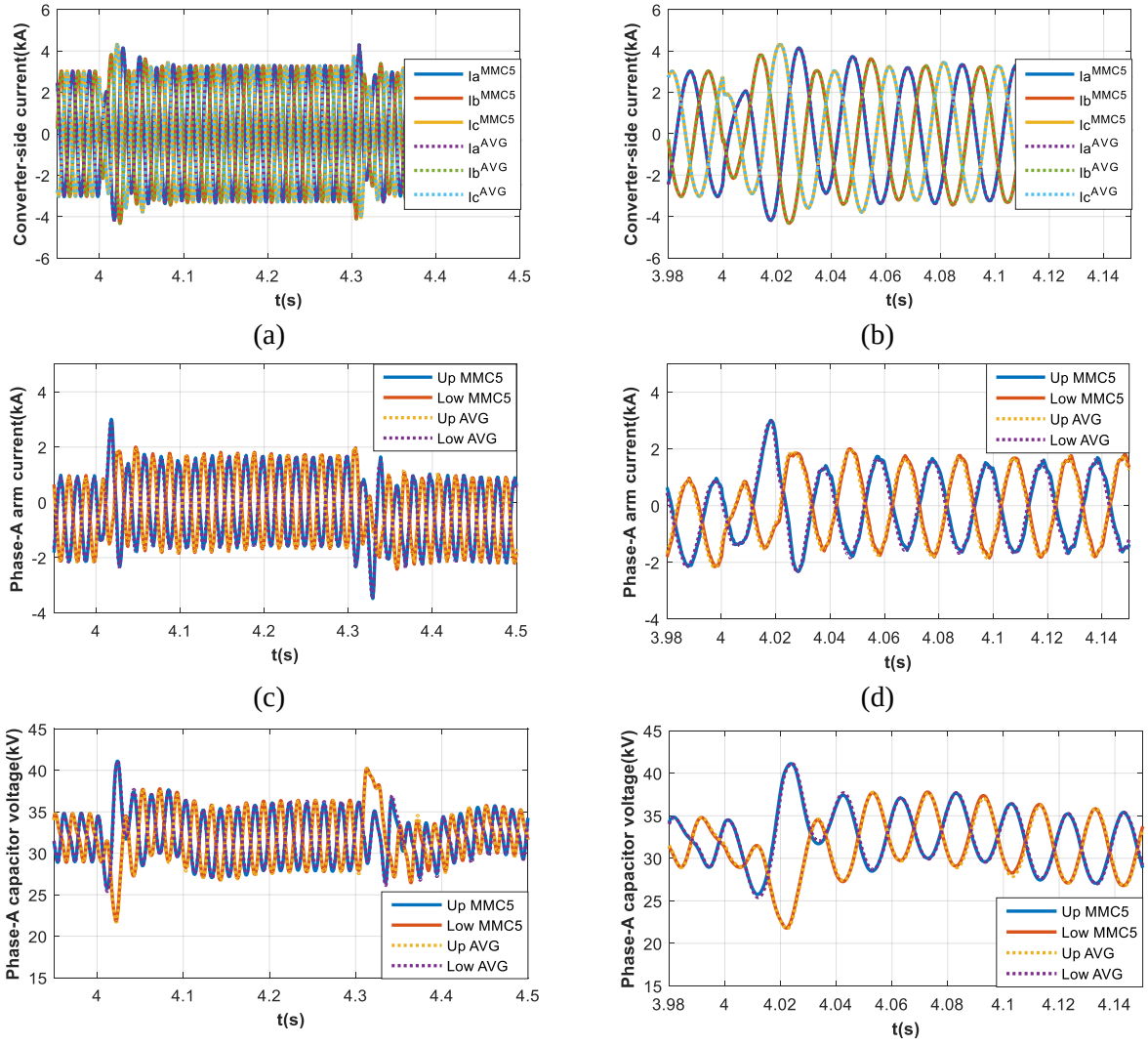

Fig. 11: Simulation waveforms that benchmark the transient behaviours of the real-time user defined averaged MMC model against that of the real-time MMC5 available in the RTDS library during a three-phase-to-ground AC fault

6 Conclusions

This report has presented a detailed validation of real-time user-defined switching function and averaged HB-MMC models against an offline validated PSCAD switching function model. Further validation of the real-time use-defined averaged HB-MMC model against benchmark averaged HB-MMC model 'MMC5' from RTDS library is presented. Detailed one-to-one comparison of the simulation waveforms (offline superimposed on the real-time) show that the offline and real-time simulation waveforms are in full agreement to the microscopic level, with the worst-case errors during AC and DC network alterations are less than 1%. On this ground, it has been concluded that the presented real-time user-defined simulation models are capable of simulating symmetrical and asymmetrical AC faults and DC faults in weak and strong AC networks with high accuracies.

7 References

[1] A. Lesnicar and R. Marquardt, "An innovative modular multilevel converter topology suitable for a wide power range," in *Power Tech Conference Proceedings, 2003 IEEE Bologna*, 2003, pp. 1-6.

[2] M. Glinka and R. Marquardt, "A new AC/AC-multilevel converter family applied to a single-phase converter," in *Power Electronics and Drive Systems, 2003. PEDS 2003. The Fifth International Conference on*, 2003, pp. 16-23 Vol.1.

[3] U. N. Gnanarathna, A. M. Gole, and R. P. Jayasinghe, "Efficient Modeling of Modular Multilevel HVDC Converters (MMC) on Electromagnetic Transient Simulation Programs," *Power Delivery, IEEE Transactions on*, vol. 26, pp. 316-324, 2011.

[4] S. Denneti, x00E, re, H. Saad, B. Clerc, E. Ghahremani, *et al.*, "Validation of a MMC model in a real-time simulation platform for industrial HIL tests," in *2015 IEEE Power & Energy Society General Meeting*, 2015, pp. 1-5.

[5] F. B. Ajaei and R. Iravani, "Enhanced Equivalent Model of the Modular Multilevel Converter," *Power Delivery, IEEE Transactions on*, vol. PP, pp. 1-1, 2014.

[6] H. Saad, Dennetie, S. J. Mahseredjian, P. Delarue, *et al.*, "Modular Multilevel Converter Models for Electromagnetic Transients," *Power Delivery, IEEE Transactions on*, vol. 29, pp. 1481-1489, 2014.

[7] J. Xu, A. M. Gole, and C. Zhao, "The Use of Averaged-Value Model of Modular Multilevel Converter in DC Grid," *IEEE Transactions on Power Delivery*, vol. 30, pp. 519-528, 2015.

[8] H. Saad, J. Peralta, S. Dennetiere, J. Mahseredjian, J. Jatskevich, J. A. Martinez, *et al.*, "Dynamic Averaged and Simplified Models for MMC-Based HVDC Transmission Systems," *Power Delivery, IEEE Transactions on*, vol. 28, pp. 1723-1730, 2013.

[9] TR on Modular Multilevel Voltage Source Converter: Fundamentals and Synthesis of Different Models, *Strathclyde-UK National HVDC Centre collaborative research project*, TR ref. USTRATH-HVDC Centre-P1-001, April 2018.